Hsf1 and the molecular chaperone Hsp90 support a "rewiring stress response" leading to an adaptive cell size increase in chronic stress

Short title: Cells adapt to chronic stress with size increase

Authors

Samarpan Maiti[1], Kaushik Bhattacharya[1], Diana Wider[1], Dina Hany[1,4], Olesya Panasenko[2], Lilia Bernasconi[1], Nicolas Hulo[3], Didier Picard[1] *

Affiliations

[1]Département de Biologie Moléculaire et Cellulaire, Université de Genève, Genève, Switzerland

[2]BioCode: RNA to Proteins Core Facility, Département de Microbiologie et Médecine Moléculaire, Faculté de Médecine, Université de Genève, Genève, Switzerland

[3]Institute of Genetics and Genomics of Geneva, Université de Genève, Genève, Switzerland

[4] On leave from: Department of Pharmacology and Therapeutics, Faculty of Pharmacy, Pharos University in Alexandria, Alexandria 21311, Egypt.

* Corresponding author: didier.picard@unige.ch

Key words

Stress adaptation, chronic stress, cell size, cytoplasmic density, Hsf1, Hsp90, aging, senescence, proteostasis, translation

Abstract

Cells are exposed to a wide variety of internal and external stresses. Whereas many studies have focused on cellular responses to acute and severe stresses, little is known about how cellular systems adapt to sublethal chronic stresses. Using mammalian cells in culture, we discovered that they adapt to chronic mild stress by increasing their size and translation, thereby scaling the amount of total protein. These adaptations render them more resilient to persistent and subsequent stresses. We demonstrate that Hsf1, well known for its role in acute stress responses, is required for the cell size increase, and that the molecular chaperone Hsp90 is essential for coupling the cell size increase to augmented translation. We term this translational reprogramming the "rewiring stress response", and propose that this protective process of chronic stress adaptation contributes to the increase in size as cells get older, and that its failure promotes aging.

Introduction

Stress has shaped the interactions between organisms and their environment since the origin of the first cell (*1*). Throughout their lifetime, cells and organisms are exposed to different kinds of environmental and cell-intrinsic stresses such as heat, genotoxic agents, oxidative agents, alterations of external pH, hypoxia, nutrient deficiency, osmotic changes, protein misfolding and aggregation, and various pathological conditions (*2*). While intense acute stresses can cause lethal damage, in a physiological environment, cells are mostly exposed to mild and often chronic stresses, so that cells have a chance to adapt (*3, 4*). For example, body or tissue temperature increases of only a few degrees constitute a mild heat stress at the cellular level (*5-9*). Similarly, the ecosystem may contain several pollutants that cause a continuous mild oxidative stress (*10*). Cells and organisms cannot easily escape such stresses and must therefore adapt.

Because cells and organisms need to live with such lifelong stresses, evolution has endowed them with highly conserved stress response pathways (*11*). Heat-shock factor 1 (Hsf1), a transcription factor, is the master regulator of cellular stress management (*12*). Hsf1 governs a protective transcriptional program known as the heat-shock response (HSR), which involves the selective transcription of stress response proteins known as heat-shock proteins (Hsps), most of which are molecular chaperones (*13-15*). Molecular chaperones collectively promote the initial folding of newly made proteins, the refolding of unfolded or misfolded proteins, the dissociation of protein aggregates, and the degradation of terminally misfolded or

aggregated, and potentially toxic, proteins (*16*). Overall, this process of maintaining protein homeostasis is known as proteostasis. During acute stress of different kinds, apart from the Hsf1-mediated transcriptional response, eukaryotic cells elicit a specific adaptive stress response, known as the integrated stress response (ISR). The ISR reprograms translation to avoid overloading the proteostasis system (*17*). In the ISR, global cap-dependent protein translation is reduced, while the translation of some proteins, needed to deal with the challenge, is specifically enhanced.

Hsps are not only required for cells to respond to stress. Even without stress, cells need a basal level of Hsps for folding nascent polypeptide chains, refolding partially denatured or misfolded proteins, or for their degradation (*18*). Hsps are categorized into different families based on their molecular weights. Among those, Hsp90 is essential for the viability and growth of eukaryotic cells and organisms, and it is a major hub of cellular proteostasis (*19-24*). It is one of the most abundant proteins in cells (*25-27*), and in mammals, a large fraction of it is indeed required during prenatal development, and for tissues and cells (*28*). In mammalian cells, there are two different cytosolic Hsp90 isoforms, which are encoded by two different genes, Hsp90α (encoded by the gene *HSP90AA1)* and Hsp90β (encoded by *HSP90AB1*) (*29*). Hsp90α is the more stress-inducible isoform whereas Hsp90β is more constitutively expressed. There are extensive overlapping functional similarities between the two Hsp90 isoforms, which are 84% identical in humans, but there is also some evidence for isoform-specific functions (*30*). However, to what extent mammalian cells require these two isoforms during stress adaptation is not clear.

Cellular stress responses, molecular chaperones, and proteostasis are interconnected with cellular and organismal aging (*21, 31, 32*). Although the process of aging is broadly influenced by genetic, epigenetic, and extrinsic factors, it is increasingly apparent that most of these factors ultimately interface with cellular stress response mechanisms (*33-35*). One of the hallmarks of aging is cellular senescence (*36-38*), which is characterized by a number of features, including a larger cell size. Earlier studies claimed that, as cells become senescent, they stop dividing. But since cell growth, defined as the addition of cell mass, continues, senescent cells become larger (*39-42*). That is why cells of older mammalian indiviuals are often two or three times larger than those of younger ones (*43-46*). Remarkably, recent studies have established that a larger cell size is not a consequence, but rather the cause of senescence. If cells fail to scale the amount of their macromolecules as they become larger, this causes cytoplasmic dilution and induces senescence (*47, 48*). The question remains why mammalian cells increase their size to the point of becoming senescent. There are a number of indications that some cells increase their size in response to external cues or functional needs (*49-52*). However, it is poorly understood whether the cell size itself is the target of regulation or a byproduct of some other adaptation (*53*).

Here we report that mammalian cells gradually enlarge their size to adapt to chronic mild stress (or "chronic stress" for short). Whereas the cellular response to acute stress has been extensively characterized (*13, 54*), little is known about how cells adapt to chronic mild stress and to what extent certain Hsps or molecular chaperones are involved. We exposed cells to several chronic stresses to investigate these issues, notably also the role of specific cytosolic Hsp90 isoforms. We

discovered that in response to chronic stress cells increase their size in an Hsf1-dependent fashion, and that their adaptation to chronic stress is different from the response to acute stress. Unlike acute stress, which causes a shutdown of global translation to reduce the protein burden, chronic stress induces global translation to increase the amount of total proteins. Hsp90, irrespective of its isoform, supports the increase in translation and, through this adaptation, the cell size increase.

Results

A mammalian cell model to study the effects of chronic mild stress

To study how mammalian cells adapt to chronic stress, we applied several stressors, such as mild heat shock (HS), hypoxia, sodium arsenite, and the protein misfolding agent L-azetidine-2-carboxylic acid (AZC), to several cell lines (Fig. 1A and fig. S1A). To gage the level of chronic stress, which we would consider mild for a given stressor, we decided that it would be the duration or the intensity, where cell death is ≤10%. To determine the chronic mild HS conditions, we kept all cell lines at different temperatures for seven days. We found the threshold for chronic HS to be 39 °C for HEK293T (HEK) and HCT116 cancer cells, and 40 °C for A549 cancer cells and the normal epithelial cell line RPE1. For hypoxia, we determined that 4 days of hypoxia (1% oxygen) are the appropriate threshold for chronic hypoxic stress. For both sodium arsenite and AZC, 5 μM for 5 days is an appropriate threshold for oxidative and proteotoxic stresses, respectively.

Chronic mild stress causes an increase in cell size

While we were checking cell death by flow cytometry to optimize the threshold for the different chronic stresses, we noticed that in all types of chronic stresses, cells increased their size over time (Fig. 1B and fig. S1B), as indicated by the forward scatter (FSC) intensity, which is proportional to the diameter (d) of the cell (*55*). Assuming cells in suspension are a round ball, note that a 10% increase in cell diameter translates to more than a 30% increase in cell volume since volume = $4/3\ \pi\ (d/2)^3$. It is well supported that mammalian cells control their size via modulation of the cell cycle (*53, 56-58*). Specifically, a lengthening of the G1 phase is responsible for cell size increases. Hence, we determined whether this increase in cell size is caused by a cell cycle arrest. After seven days of chronic HS, we checked the cell cycle profiles of HEK and A549 cells (Fig. 1C). Interestingly, the two cell lines showed different cell cycle patterns in chronic HS. While A549 cells have a slightly increased G1 population, HEK cells maintain a similar cell cycle profile. We repeated the analyses at different time points of chronic HS and found that at the initiation of chronic stress, there is a substantial number of cells in the G1 population for both cell lines (Fig. 1D). Over time, the cell cycle stabilizes in a cell line-specific fashion, suggesting that cells are able to adapt to chronic HS. Importantly, despite the stabilization of the cell cycle during continued chronic stress, cells maintain an enlarged cell size (Fig. 1E) with an almost equal proliferation rate (Fig. 1, F and G, and fig. S1C) in the beginning of the stress or after 7 days of stress adaptation. To check if this cell size enlargement is reversible, we put the cells back at 37°C after 7 days of chronic HS. During this recovery period at 37°C, both HEK and A549 cells returned to their usual size (Fig. 1H), and A549 cells also reverted back to a normal cell cycle profile (Fig. 1I and fig. S1D).

A minimal level of Hsp90 is required for chronic stress adaptation

A key question is how cells cope with and adapt to these chronic stresses. A complex network of molecular chaperones and their respective co-chaperones acts as a buffer to the myriad of changes during stress (*3, 13, 31, 59*). The cytosolic Hsp90 isoforms are the most abundant molecular chaperones (*60-63*). Since Hsp90 had been found to support the size increase of cardiomyocytes following myocardial infarction (*64*), we wondered whether it plays any role in the stress-induced cell size increase, and if so, which one of the two cytosolic Hsp90 isoforms, that is Hsp90α or Hsp90β (*30*). To address this, we used our human Hsp90α knockout (KO) and Hsp90β KO HEK and A549 cells (Fig. 2A) (*28*). Note that hereafter we will refer to cells lacking one *or* the other isoform as Hsp90α/β KO cells. We observed that the loss of either one of the two isoforms makes them vulnerable to different chronic stresses (Fig. 2B and fig. S2A). However, even in the absence of one Hsp90 isoform, cells enlarged their size during chronic HS, and hypoxic and oxidative stress conditions (Fig. 2, C and D, and fig. S2, B and C). This suggests that the stress-induced cell size increase is not directly associated with a particular cytosolic Hsp90 isoform.

The canonical Hsf1 activity regulates the cell size increase in response to chronic stress

Hsf1 is an evolutionarily conserved transcription factor that mediates the cytoprotective HSR throughout the eukaryotic kingdom (*65, 66*). It is well established that Hsf1 activity increases in response to acute stresses (*12*). During stress,

mammalian Hsf1 monomers in the cytosol are activated to form trimers, which localize to the nucleus, bind DNA sequences known as heat shock elements (HSE), and trigger the transcription of target genes (*14*). It has been proposed that Hsp90 controls Hsf1 activity by titrating Hsf1 under non-stress conditions (*67-71*). Using an Hsf1 reporter plasmid, we found that Hsp90α/β KO cells, and most prominently Hsp90α KO cells, have a higher basal level of Hsf1 activity (Fig. 3A). In Hsp90α/β KO cells, the higher basal Hsf1 activity could be due to a larger number of Hsp90-free Hsf1 molecules. We did observe that there is more Hsf1 in the nucleus of Hsp90α/β KO cells in non-stressed conditions (Fig. 3B), and yet Hsf1 becomes even more nuclear in cells of all three genotypes during chronic HS (Fig. 3B). This also translates to a higher Hsf1 activity, as we could observe with a Hsf1 reporter assay (Fig. 3C). To characterize the proteomic changes associated with Hsp90α/β KO and chronic HS, we performed quantitative label-free proteomic analyses of cells maintained in non-stressed conditions, and after one day and four days of HS. The proteomic data confirmed the increased basal Hsf1 activity that we had seen in Hsp90α/β KO cells with the Hsf1 reporter assay. Many proteins whose expression was known to be regulated by Hsf1 proved to be upregulated in Hsp90α/β KO cells (fig. S3A and data S1). Under chronic HS, cells of all three genotypes were able to increase the expression of several Hsf1 target genes (Fig. 3D), reminiscent of what we had seen with the Hsf1 reporter assay. Thus, cells are perfectly capable of mounting a HSR in the absence of either one of the two Hsp90 isoforms, suggesting that their increased vulnerability to stress may be due to something else.

To obtain more direct experimental evidence for a role of Hsf1 in the cell size increase induced by chronic HS, we overexpressed WT Hsf1 and a transcriptionally defective Hsf1 mutant in HEK, A549, and RPE1 cells. We observed a strong induction of basal Hsf1 activity in cells overexpressing WT Hsf1 but not the mutant form (fig. S3B), correlating with an increase in cell size under normal non-stress conditions (Fig. 3E). Taken together, our observations suggest a correlation between the canonical transcriptional Hsf1 activity and cell size. We further strengthened this correlation by determining the effect of inducing Hsf1 activity pharmacologically with capsaicin, which is known to trigger a calcium influx and HSR through the vanilloid receptor TRPV1 (*72, 73*). We found that A549 cells of all three genotypes display a capsaicin-induced and dose-dependent transcriptional Hsf1 activity (fig. S3C) and cell size increase (fig. S3D). Collectively, these results indicate that the transcriptional Hsf1 activity is sufficient to cause a cell size increase. To determine whether Hsf1 is necessary for the cell size increase, we used RNA interference to knock down Hsf1 expression in A549 WT and Hsp90α KO cells (fig. S3E). Hsf1 knockdown cells exposed to chronic HS failed to display Hsf1 activity (fig. S3F), and could not increase their cell size during adaptation to chronic HS (Fig. 3F).

So far, we have only shown results obtained with established human cell lines. We also explored the link between Hsp90 and Hsf1 activity in mouse adult fibroblasts (MAFs) established from mice with only a single allele for cytosolic Hsp90 left. These are both homozygous *hsp90α* KO and heterozygous *hsp90β* KO, and will be referred to as 90αKO 90βHET (*28*). These MAFs proved to be substantially bigger than WT MAFs (fig. S3G), and to display a several-fold higher basal Hsf1 activity (fig. S3H). It

should be emphasized that these MAFs were obtained from adult mice that had escaped the stringent developmental attrition of embryos with this genotype through translational reprogramming of Hsp90β expression (*28*). This may explain why these mutant MAFs, unlike WT MAFs, could not augment their Hsf1 activity nor increase their size any further in chronic HS (fig. S3, I and J). At this point, we conclude that the HSR correlates with cell size during chronic stress, and that both outcomes are mediated by Hsf1.

Hsp90α/β KO cells overall maintain their chaperome and proteome complexity during chronic stress

Under normal physiological conditions, cells maintain proteostasis through a complex network of molecular chaperones and co-chaperones, a protein collective referred to as the cellular chaperome (*74, 75*). Cellular adaptation to stress does not only require increased Hsf1 activity, but it is also modulated by complex functional relationships between Hsf1 and the cellular chaperome (*12*). Even though the HSR in chronic stress is not impaired by the loss of one of the Hsp90 isoforms, Hsp90α/β KO cells gradually die off during the chronic HS adaptation period (Fig. 2B). This raises the question whether the chaperome is compromised in the absence of Hsp90α or β. Using the proteomic data sets mentioned above, we focused on the protein levels of all molecular chaperones and co-chaperones at 37°C and in chronic HS at different time points. This analysis revealed that Hsp90α/β KO cells could still maintain or increase expression of molecular chaperones and co-chaperones during chronic HS (Fig. 4A). Immunoblots confirmed the upregulation of the heat-inducible molecular chaperones Hsp90α, Hsp70, Hsp40, and Hsp27 throughout the chronic

stress in cells of all three genotypes (Fig. 4B and fig. S4A). This suggests that the chaperome of Hsp90α/β KO cells is not compromised by chronic stress. Similarly, at the whole proteome level, standardized to the same amount of protein, and although there are genotype-specific differences, the proteome remained complex during chronic stress indicating that proteostasis was largely intact (fig. S4B). Next, we analyzed the Hsp90 interactome. We found that the Hsp90α or Hsp90β KO cells could largely maintain the Hsp90 interactors throughout the chronic stress. These data demonstrate that one Hsp90 isoform is sufficient to support most interactors (Fig. 4C and fig. S4, C and D).

To address the protein folding ability of Hsp90α/β KO cells more directly, we performed an *in vivo* refolding assay with exogenously expressed firefly luciferase subjected to unfolding by a short HS at 43 °C. Surprisingly, we found that Hsp90α/β KO cells do even better than WT cells under basal conditions (37° C) (Fig. 4D). The KO cells also showed an increased luciferase refolding ability when they were cultured for 2 days at 39 °C prior to luciferase unfolding (Fig. 4E). This higher refolding activity of the Hsp90α/β KO cells at 37° C might be due to some other molecular chaperones being more highly expressed than in WT cells (Fig. 4B). Similarly, Hsp90α/β KO cells might do better than WT cells under chronic HS because of their ability to further increase the levels of other molecular chaperones, such as Hsp27, Hsp40, and Hsp70, during chronic HS. So far, these observations suggest that a reduced level of Hsp90 is at least in part functionally compensated by other molecular chaperones in these assays.

A normal level of Hsp90 is required to maintain the cytoplasmic protein density in chronic stress

If Hsp90α/β KO cells do as well or even better than WT cells for almost all parameters investigated so far, what causes them to be more sensitive to stress (Fig. 2B)? It is known that when cells grow larger, it is critical for them to maintain a constant cellular protein concentration (*48, 76-78*). To achieve this, cells need to increase the total amount of proteins proportionately to their size increase (*47*), a process that can be referred to as scaling. Uncoupling of protein synthesis and cellular volume causes a dilution of the cytoplasm, which results in cellular senescence and aging. We tested cytoplasmic density by measuring the mobility of EGFP *in vivo* using fluorescence recovery after photobleaching (FRAP) experiments (fig. S5A). We calculated the t-half values and diffusion rates (*17*), and found that only WT cells could maintain the same cytoplasmic density under chronic HS as at 37 °C (Fig. 5A and fig. S5, B to D). Hsp90α/β KO cells of both cell lines showed lower t-half values and higher diffusion coefficients in chronic stress indicating that they have a reduced cytoplasmic density (Fig. 5A and fig S5, B to D). This observation suggests that a full complement of cytosolic Hsp90 is necessary to maintain the cytoplasmic density with the increase of cell size in chronic stress. There is no significant difference between Hsp90α/β KO cells, which indicates that total Hsp90 levels rather than a specific isoform are critical for maintaining the cytoplasmic density.

If the cytosol is more diluted, this should be reflected in the total amount of proteins. Therefore, we collected the same number of non-stressed and stressed enlarged

cells after one day and four days of chronic HS, lysed them in the same amount of lysis buffer, and measured the protein concentrations in the lysates. We found that after four days of chronic stress, the total amount of proteins was higher in WT cells, whereas it decreased in Hsp90α/β KO cells (fig. S5E). Quantitation by flow cytometric analysis of total cellular protein stained with an amine-reactive dye revealed qualitatively similar results. The total amount of proteins per cell increased with cell size in WT but not in Hsp90α/β KO cells (Fig. 5B and fig. S5E). These results demonstrate that cells are unable to maintain the ratio of total protein to cell size in chronic stress when Hsp90 levels are reduced.

Normal levels of Hsp90 are required to scale protein biosynthesis during stress-induced cell size enlargement

One of the key features of the acute stress response of mammalian cells is a global inhibition of translation (*79-82*). We demonstrated here that WT cells exposed to chronic stress increase the total amount of proteins as they get larger, raising the question of how they do it. Revisiting our proteomic data set, we saw that the levels of ribosomal proteins are least reduced in WT compared to Hsp90α/β KO cells under chronic stress (Fig. 5C). A reduction of the core machinery of translation may explain why Hsp90α/β KO cells have decreased amounts of total proteins compared to WT in chronic stress. However, it does not explain the observation of the increased amount of total proteins in WT cells under chronic stress. To address this issue, we checked global translation by labelling nascent polypeptide chains with a fluorescent version of puromycin, which allows measurements for individual cells by flow cytometry. We saw a strong increase of labelled nascent polypeptides in WT cells

both on day 1 (fig. S5F) and day 4 (Fig. 5D) of adaptation to chronic HS. By comparison, Hsp90α/β KO cells failed to maintain the same rate of protein biosynthesis under chronic HS (Fig. 5D and fig. S5F). While the stress-adapted bigger cells have a higher level of total translation (Fig. 5D), it is known that acute HS causes ribosomal dissociation from mRNA, which results in a translational pause (*80*). Polysome profiling of WT cells adapted to stress for four days showed that the polysome profiles of cells grown at 37 °C or in chronic HS are largely similar (Fig. 5E). Similar peaks of single ribosomal particles (40S and 60S), monosomes (80S), and polysomes (both small and large) suggest that the association of ribosomes and mRNAs in WT cells is not affected during adaptation to chronic stress. This raises the question of whether the ISR is not triggered when the stress is chronic. To address this, we did puromycin labeling at earlier time points of chronic HS. We observed that at the beginning of chronic stress (4 h), reminiscent of the ISR (*17*), translation is reduced as seen by flow cytometry (fig. S5G) and puromycin labelling of nascent chains detected by immunoblotting (fig. S5H). Moreover, cells of all three genotypes displayed an increased inhibitory phosphorylation of the eukaryotic translation initiation factor 2A (eIF2α), a hallmark of the ISR (*83, 84*), after 4 h of HS (Fig. 5F and fig. S5I). After having been exposed to chronic HS for one day and more, cells increase total translation, to an even higher level than the basal translation at 37 °C (fig. S5G), consistent with the higher translation rate observed by puromycin labeling of nascent chains (Fig. 5D and fig. S5F). As cells remained in chronic HS, the phosphorylation of eIF2α only dropped in WT but not Hsp90α/β KO cells. These findings indicate that at the very beginning of chronic HS, an ISR is induced with the accompanying inhibitory phosphorylation of eIF2α and global

reduction of translation. WT cells but not Hsp90α/β KO cells, once adapted to the stress, recover normal or even increased global translation. Translational recovery of WT cells is also reflected in several other translation markers and regulators. We could see an increase in the phosphorylation of mTOR, 4EBP1, and S6 during adaptation to chronic HS (Fig. 5G and fig. S5I). Thus, it is primarily this recovery, which constitutes a critical and Hsp90-dependent aspect of stress adaptation.

The mTOR complex 1 (mTORC1) is known to regulate cell size by regulating cellular translation (*85*). Hsf1 in a non-transcriptional mode has been linked to regulating organ and cell size by preserving mTORC1 activity (*86*). And yet, we saw that Hsp90α/β KO cells increase their size in chronic HS despite failing to augment global translation. We therefore determined cell size and translation at different time points following exposure to chronic HS (Fig. 5H). In contrast to WT cells for which cell size and translation appear to be coupled, Hsp90α/β KO cells increase cell size while translation is still reduced. Thus, cell size and translation must be coupled for adaptation to chronic stress. It remains to be seen how Hsp90α/β KO cells manage to increase their size without a concomitant scaling of translation and to what extent the mTORC1-mediated regulation of translation is involved.

Hsp90α/β KO cells are efficient at maintaining cellular proteostasis under normal unstressed conditions

In experiments presented above, we showed that the loss of one Hsp90 isoform does not impair the protein refolding ability (Fig. 4, D and E), but reduces translation under chronic stress. Proteolysis is complementary to translation and folding, and

crucial to prevent cytotoxicity by eliminating damaged proteins (*32*). Cells promote the degradation of terminally misfolded proteins via the autophagy-lysosomal pathway (ALP) or the ubiquitin-proteasome system (UPS) (*87, 88*). We performed an *in vivo* activity assay for the UPS, which involved the transient expression and flow cytometric quantitation of a degradation-prone ubiquitin-GFP fusion protein (Ub-R-GFP) and its stable counterpart (Ub-M-GFP) as a control (*89*). We observed no significant differences in the UPS activity of Hsp90α/β KO cells compared to WT cells at 37 °C (fig. S6A). We checked the ALP by measuring the autophagic flux using a mCherry-GFP-LC3 reporter (*90*). Here also, we observed that the autophagic flux remains unchanged in Hsp90α/β KO cells (fig. S6B). These results lead us to conclude that one Hsp90 isoform is sufficient to maintain cellular proteostasis under normal, unstressed conditions.

A normal level of Hsp90 is required to maintain cellular proteostasis in chronic stress

We recently reported that Hsp90α/β KO HEK cells accumulate insoluble proteins in long-term mild HS (*28*). We therefore checked the above-mentioned cellular proteostasis axes after four days of adaptation to chronic stress. We found that the absence of either one of the two Hsp90 isoforms causes a deficit in UPS activity *in vivo* (Fig. 6A) and autophagic flux (Fig. 6B). Hsp90α/β KO cells subjected to chronic HS also had reduced proteasomal activity when measured *in vitro* (Fig. 6C). When we expressed the aggregation-prone model protein EGFP-Q74 (*91*) in stress-adapted Hsp90α/β KO cells, large aggregates of EGFP-Q74 were readily detectable (Fig. 6D). This suggests that Hsp90α/β KO cells cannot efficiently maintain

proteostasis in chronic stress. Since Hsp90α KO and Hsp90β KO cells are largely affected the same way, we conclude that there is no isoform specificity for maintaining proteostasis during stress, but that total Hsp90 levels above a certain threshold might be the critical parameter.

Enlarged cells are more resistant to subsequent stress

We hypothesized that the stress-induced cell size enlargement is a protective adaptation. To address this, we induced the enlargement or reduction of cell size with different inhibitors and examined how cell size affects cell survivability (Fig. 7A). At first, we enlarged the A549 WT and Hsp90α/β KO cells by treating them with a CDK4/6 inhibitor (Fig. 7B), which is known to promote a G1 arrest-associated increase in cell size (*47*). In contrast to what we had seen with chronic HS, upon becoming bigger in response to treatment with the CDK4/6 inhibitor, Hsp90α/β KO cells were able to scale the amount of total proteins (fig. S7, A and B). This demonstrates that scaling total protein is possible even in the absence of one Hsp90 isoform and a reduced amount of total Hsp90 when cells are not in chronic HS. We showed above that Hsp90α/β KO cells were dying in chronic HS, possibly because they could not scale their protein with increasing cell size. We therefore wondered whether Hsp90α/β KO cells, enlarged with prior treatment with the CDK4/6 inhibitor, might be more resistant to chronic HS because they would already have scaled their total protein. After treatment with CDK4/6 inhibitors for three days, we washed off the inhibitors and subjected the cells to chronic HS for three days. We observed that cells that were already enlarged due to the CDK4/6 inhibitor treatment did not get even bigger in chronic HS. As predicted, these pre-enlarged Hsp90α/β KO cells were

more resistant and less prone to apoptosis and cell death (Fig. 7B). Thus, when given a chance to get bigger with protein scaling, even cells lacking one Hsp90 isoform are more resistant to chronic stress.

We further explored the connection between increase in cell size and scaled protein, and stress resistance with other stresses and cell lines. We treated the cells pre-enlarged with the CDK4/6 inhibitor with an acutely toxic concentration of sodium arsenite for one day. Again, pre-enlarged A549 cells of all three genotypes and the normal RPE1 cells were more resistant to this subsequent stress (fig. S7C). We then wondered whether reducing cell size would have the opposite effect. We treated HEK and A549 WT, and Hsp90α/β KO cells with rapamycin to inhibit mTOR-induced cell growth (*85*) (Fig. 7C and fig. S7D). Cell size was indeed reduced after three days of rapamycin treatment (Fig. 7C and fig. S7D). Surprisingly, we found that even in the presence of rapamycin cells enlarged their size under chronic HS, albeit not up to the level of cells without rapamycin pretreatment. More of these comparatively smaller rapamycin-treated WT cells were apoptotic than of the bigger cells not treated with rapamycin (Fig. 7C and fig. S7D). The increased cell death could also be due to the translational inhibition, in light of the fact that WT cells display increased total translation and mTOR activity to adapt to chronic stress (Fig. 5G and fig. S5I). In contrast, we observed that comparatively smaller rapamycin-treated Hsp90α/β KO cells were less prone to apoptosis than the non-treated bigger cells. It remains to be seen whether the ratio of total protein to cell size is slightly more favorable in Hsp90α/β KO cells under these conditions. To further support the importance of mTOR, we treated the larger cells adapted to chronic HS with rapamycin. We

observed that WT cells became more apoptotic when we added rapamycin after three days of stress adaptation (Fig. 7C and fig. S7D). As rapamycin pre-treatment failed to restrict the cell size increase caused by chronic stress, we then tried to limit the cell size increase with serum starvation (fig. S7E). We observed that even serum-starved cells enlarged their size in additional chronic stress as they did with rapamycin. Here again, the size enlargement was not up to the level of non-starved cells. We observed that the serum-starved smaller WT cells died more under stress than the non-starved bigger cells (fig. S7E). As with the rapamycin treatment, in most cases, the serum-starved smaller Hsp90α/β KO cells survived better than the bigger non-starved cells. In both experiments, we did not succeed in preventing the cell size increase upon exposing cells to chronic HS. As a control experiment, we subjected smaller cells obtained with cycloheximide or rapamycin treatment to an acute stress with arsenite for one day. We found that smaller cells were more sensitive to acute stress irrespective of Hsp90 isoform and levels (fig. S7F).

We then wondered what would happen if we limited the cell size increase by limiting the available space (Fig. 7D). We used RPE1 cells, as these cells always grow in single layers and do not grow on top of each other once they are entirely confluent. We observed that at 37°C, once they become confluent, they do not stop dividing, but become smaller and smaller (Fig. 7, E and F). In contrast, in chronic HS, over time, they enlarge their size and keep dividing when seeded at low density. Next, we seeded a comparatively higher number of cells, such that the culture plate would already be confluent from the beginning, and put it in chronic HS. We observed that the cells in the 'already-confluent' plate at 37 °C kept dividing and shrinking, without

obvious cell death (Fig. 7, E and F). However, in chronic HS, the cells in the 'already-confluent' plate, while they were initially able to enlarge their size to some extent, when their size eventually shrank because of the limited space, they started dying off (Fig. 7F).

Adaptation to chronic stress requires cytosolic Hsp90 above a threshold level irrespective of Hsp90 isoform

So far, our experiments did not reveal any obvious functional differences between the two cytosolic Hsp90 isoforms. This supports the conclusion that the observed phenotypes in chronic stress, rather than being linked to a specific isoform, are due to below threshold levels of total Hsp90. To address this more directly, we exogenously overexpressed Hsp90α or Hsp90β as mCherry or EGFP fusion proteins, respectively, in Hsp90α/β KO cells. This caused an overall increase in total Hsp90 levels (Fig. 7G). The transfected cells were subjected to chronic HS. After four days, we checked the scaling of total protein by loading an equal volume of cell lysate on a protein gel (see Materials and Methods for details). We found that when the total levels of Hsp90 are elevated by either one of the two isoforms, Hsp90α/β KO cells are able to scale total protein under chronic HS (Fig. 7G).

Discussion

It is now increasingly recognized that exposure to mild environmental stressors is not necessarily detrimental to the organism. Instead, such experiences may foster a

resistant or adapted phenotype through hormesis (*92*). Hormesis is a core mechanism of developmental plasticity by which an organism's response to a stressor varies with exposure (*93*). In contrast, hormetic priming is confined to specific temporal windows and can be considered a preparation to cope with stress. The biological process of aging is claimed to be associated with hormesis (*94*). Therefore, physiological cellular responses to mild rather than severe stresses may be more important to address in order to comprehend the biology of aging.

Cell size enlargement is a prerequisite for chronic stress adaptation

We report that cells adapt to chronic stress by gradually enlarging their size, through a process coupled with increased translation. Stress-induced cell size enlargement is a step towards stress adaptation as part of an intrinsic stress response. Even when we used inhibitors known for restricting the cell size, chronic stress still induced a cell size increase (Fig. 7 and, fig. S7). This suggests that cell size enlargement is a necessity for cells to adapt to prolonged stress. Cell size enlargement has also been linked to cellular senescence, which is a state of long-term cell cycle arrest (*36-38*). In contrast, stress-adapted bigger cells continue to proliferate. It has been reported that bigger cells, when they cannot scale their cellular macromolecules, suffer from cytoplasmic dilution and become senescent (*47*). The adaptive cell size enlargement in response to chronic stress is coupled with increased translation, which enables cells to maintain their cytoplasmic density and macromolecular crowding. Maintaining macromolecular crowding is necessary to control the kinetics of cellular reactions and to avoid an aging-related deterioration of cellular biochemical processes (*95*). Hence, the adaptive cell size increase in response to chronic stress is different from

that associated with cellular senescence. Our observations demonstrate that the coupling of cell size enlargement and translation is essential for cells to adapt to chronic stress. Failure to do so causes their elimination during stress exposure, as we observed with Hsp90-deficient cells.

Hsp90 enables the rewiring of the stress response

Hsp90-deficient cells subjected to chronic stress suffer from cytoplasmic dilution. For long-term survival under intrinsic or environmentally imposed chronic stress, cells must maintain an equilibrium of protein synthesis, maintenance, and degradation (*31, 32*). Our results indicate that Hsp90 is a key molecule for sustaining translation under these conditions. Unlike during the ISR, in which global cap-dependent protein translation is specifically reduced by the hyperphosphorylation of eIF2α (*17, 96*), during adaptation to chronic stress, we observed a different phenomenon, which we term "rewiring stress response" (RSR). During RSR, cells initially reduce global translation as happens during an ISR. Then, they turn global translation back on, even when they continue to be exposed to the same stress. This leg of the response requires a threshold level of Hsp90. A hallmark of these transitions is the phosphorylation status of eIF2α and its accompanying impact on global translation. At the beginning of a chronic stress, eIF2α is hyperphosphorylated and global translation is inhibited, whereas prolonged exposure to chronic stress results in the reduction of eIF2α phosphorylation and resumption of translation (Fig. 5, D to F, and fig. S5, F to I). Thus, the dephosphorylation of eIF2α is central to this phase of the RSR, as it is to terminating the ISR (*84*). While WT cells switch translation back on, the status of eIF2α phosphorylation and puromycin labeling show that Hsp90α/β KO

cells are unable to support this transition, even though they continue to express stress-inducible chaperones and co-chaperones at high levels (Fig. 4). It appears that Hsp90-deficient cells are stuck at the ISR stage of the RSR. While the ISR is a powerful survival strategy in acute stress, it fails to support the survival of Hsp90-deficient cells during chronic stress adaptation. The ability to mount a RSR is pivotal for the adaptation of cells to chronic stress. The translational recovery and the expression of some of the stress-inducible genes in response to acute stress of the endoplasmic reticulum and oxidative stress depend on protein phosphatase 1 (PP1) and its regulator GADD34 (*97-99*). However, our proteomic data indicated that there are no significant changes of PP1 or GADD34 protein levels when one compares cells of different genotypes and stress conditions. Hence, what factors and mechanisms allow cells to transition to RSR remains to be discovered. We report here that a threshold level of total Hsp90 is important to turn on the RSR, not the presence of a particular Hsp90 isoform. If one experimentally elevates the levels of either one of the isoforms, cells can activate the RSR (Fig. 7G).

Larger cells may be more stress-resistant because of above-threshold levels of macromolecules

When acute stress triggers the ISR, cells only translate selected proteins. With persistent intense stress, the ISR cannot support proteostasis and shifts cells toward apoptosis (*100*). When stress is chronic, cells need more than this limited set of proteins. This is where the RSR comes in, allowing cells to get bigger, and to accumulate more protein molecules, and potentially other macromolecules, per cell. It is conceivable that there is an evolutionarily optimized range or a minimal threshold

level for all macromolecules, and that this depends on the specific biological needs of a given cell type subjected to a particular type of stress (Fig. 7H). If the absolute numbers per cell of certain molecules are more important than concentration to adapt and to survive under chronic stress, then bigger cells, which have larger stocks of those molecules, may be better at coping with limited damage than smaller cells. This may even apply to proteins involved in translation, including ribosomal proteins, which did not fully scale even in WT cells. As long as individual cells are above the threshold levels for all relevant macromolecules, they can adapt. Hence, growing bigger is an adaptive response that confers higher stress resistance.

This notion is also supported by our recent findings with mouse KOs (*28*). When we reduced the number of alleles for the cytosolic Hsp90 isoforms from four to one, only embryos that could reestablish the threshold levels of Hsp90 protein by translational reprogramming survived and displayed no apparent phenotype, despite the fact that Hsp90 levels were still lower than those of WT littermates (*28*). There is also evidence that cells can maintain favorable macromolecular crowding by reducing the concentration of highly abundant proteins. The mTORC1 pathway modulates the effective diffusion coefficient within the cytoplasm by reducing the number of ribosomes (*101*). This can avoid increasing molecular crowding, which has been shown to hinder the kinetics of biochemical reactions (*95, 102-104*). Increased macromolecular crowding might affect protein folding, final shape, conformational stability, binding of small molecules, enzymatic activity, protein-protein interactions, protein-nucleic acid interactions, and pathological aggregation (*105*). Hence, cells that are exposed to prolonged proteotoxic stress might try to maintain a threshold of

all the required proteins instead of scaling all proteins at a particular concentration, while tuning molecular crowding to maintain optimal cytoplasmic diffusion coefficients.

Hsf1-dependent cell size enlargement drives the activation of translation in chronic stress

We found that cell size enlargement during chronic stress depends on Hsf1 activity. This is reminiscent of prior evidence that demonstrated that Hsf1 is linked to the regulation of cell size in different tissues in mammals (*86, 106-108*). Hsf1 had been reported to maintain cell growth in a noncanonical way by preserving mTORC1 activity and translation by binding and inactivating the kinase JNK, a known inhibitor of mTORC1 activity (*86*). In contrast, the cell size increase in response to chronic stress appears to be a canonical Hsf1-mediated HSR phenomenon, which is upstream and independent of the scaling of cellular translation. This is supported by several experiments. Hsp90α/β KO cells subjected to chronic stress could increase their size despite reduced translation. Chronic stress still induced an increase of cell size upon inhibition of translation with rapamycin or cycloheximide, or by serum starvation (Fig. 7 and fig. S7). We conclude from all of these observations that increased translation is not necessary for cells to increase their size under chronic stress. WT cells start enlarging their size as a response to chronic stress and then translation follows to scale total protein levels. Hsp90α/β KO cells also increase their size in response to stress but fail to couple that to translation, which causes cytoplasmic dilution.

Aging as a failure to adapt to chronic stress

Overall, our findings are relevant to understanding aging. It is well established that mammalian cells get bigger as they grow older (*43-46*). We speculate that cells enlarge their size with aging as a protective adaptation to accumulating intra- and extracellular stressors. As long as cells manage to scale the biosynthesis of macromolecules such as proteins, their increasing size mitigates the impact of aging. Eventually, the accumulation of stressors cannot completely prevent the development of features of aging.

Our findings may have implications for rejuvenation therapies aimed at delaying or even reverting cellular aging (*109*). Treatment with the mTORC1 inhibitor rapamycin has been reported to improve the function of aged cells and to lengthen the life span of laboratory animals (*110-112*). Despite the low doses that are experimentally used to prevent an age-related decline, there are several adverse side effects. Our data indicate that treatment with mTORC1 inhibitors should be personalized based on the cellular stress level. For healthy cells, where translation plays a vital role in chronic stress adaptation, long-term treatment with rapamycin might affect cellular homeostasis and precipitate aging, or even induce apoptosis. For aged cells with a weakening proteostatic system, rapamycin may rejuvenate cells by reducing translation and inducing autophagy. This is supported by our observation that Hsp90α/β KO cells, where proteostasis is compromised, rapamycin treatment helped the cells to survive better under chronic stress (see also ref.*28*). We conclude that rather than running the risk of inducing premature aging with prolonged rapamycin

treatment from a relatively early age, efforts should focus on developing compounds that induce Hsp90 expression and/or activity, which one could expect to delay aging.

Physiological changes of cell size

Our observations demonstrate that changes of cell size do not have to be the result of physical constraints, but can be a regulated adaptation. There is evidence for changes in cell size that are induced by physiological conditions (*53*), and, of course, aging would be one of them. For example, for rat pancreatic β-cells, insulin secretion, metabolic activity, and global protein production rates are positively correlated with cell size (*113*). In the kidney, epithelial cells modulate their size in response to fluid flow rates (*49*). Muscle fibers increase their size in an Hsf1-mediated response to heat generated by exercise (*108*). Hsf1 null mice cannot increase the size of their skeletal muscle cells (*107*). Furthermore, Hsf1 plays a critical role in the adaptive increase of the size of cardiac cells (*106*). In many organs, when cell numbers decrease due to aging, this is compensated by an increase in cell size to maintain the overall functional capacity (*53*). Pancreatic β cells increase their size by over 25% during pregnancy in response to increased insulin demand (*50*). Similarly, the size of the liver increases during pregnancy through hepatocyte hypertrophy (*114*), and liver organ and cell size undergo circadian oscillations (*115*). Hepatocyte size was also found to increase in organisms continuously exposed to toxic environments (*51*). These examples support the idea that it is advantageous for a specific cell type to adopt a specific size under particular physiological conditions. Based on our findings with chronic stress, it would be worth

investigating whether Hsp90 more generally supports translational scaling in the context of these physiological changes in cell size.

Limitations of this study

Hsf1 mediates the cell size increase stimulated by chronic stress, but how chronic stress is sensed and relayed to Hsf1 remains to be established. The underlying mechanism may not be exactly the same as the one involved in mediating acute stress, which itself remains poorly understood. Furthermore, how Hsf1 induces the cell size increase is unknown, and the role of Hsp90 in stimulating translation needs to be dissected in more detail.

Materials and Methods

Cell lines and cell culture

Human embryonic kidney HEK293T cells (ATCC, CRL-3216), A549 human lung epithelial carcinoma cells (ATCC, CCL-185) (as well as the corresponding Hsp90α/β KO cell lines), and RPE1 human retinal epithelial cells (ATCC, CRL-4000), HCT116 human colon carcinoma cells (ATCC, CCL-247) were maintained in Dulbecco's Modified Eagle Media (DMEM) supplemented with GlutaMAX (Thermo Fisher Scientific #31966047), 10% fetal bovine serum (FBS) (PAN-Biotech #P40-37500), and penicillin/streptomycin (100 u/ml) (Thermo Fisher Scientific #15070063) with 5% CO_2 in a 37 °C humidified incubator. We have previously established and characterized MAFs (*28*). Experiments related to MAFs were performed with the cells at 12–24 passages. Human Hsp90α (*HSP90AA1*) and Hsp90β (*HSP90AB1*) KO

HEK and A549 cells were generated by the CRISPR/Cas9 gene-editing technology, as reported earlier (*22, 28*). For transient transfections, cells were initially seeded at 2×10^5 per 2 ml in 6-well plates and transfected using PEI MAX 40K (Polysciences Inc. # 24765-100) (1:3 DNA to PEI ratio), except for A549 and its corresponding Hsp90α/β KO cell lines. For transient transfection of A549 cells, Lipofectamine LTX (Invitrogen #15338030) was used as directed in the manufacturer's protocol. Cell culture media were changed after 6-8h of transfection. Additional chronic stress or treatments were applied 24 h after transfection.

Plasmids

For the transient overexpression of WT and mutant Hsf1, plasmids pcDNA-Flag HSF1 wt and pcDNA-Flag HSF1 C205, respectively, were used (a gift from Len Neckers (*71*)). The plasmid pcDNA-Flag HSF1 C205 allows expression of the Hsf1 mutant comprising only the N-terminal 205 amino acids. pcDNA3.1(+) (Thermo Fisher Sci. # V79020) was used as the empty vector control. For transient overexpression of Hsp90α and Hsp90β, plasmids pCherry.90α, and pEGFP.90β were used (*116*). pmCherry-C1(*116*) and pEGFP-C1 (Clontech #6084-1) were used as respective vector control. The autophagy reporter plasmid FUW mCherry-GFP-LC3 was a gift from Anne Brunet (Addgene #110060) (*90*). Plasmids Ub-M-GFP and Ub-R-GFP were a gift from Nico Dantuma (Addgene #11939) (*89*). The Hsf1 reporter plasmid HSE (WT)-Luc was a gift from Ueli Schibler (*117*). Plasmid pEGFP-Q74 was a gift from David Rubinsztein (Addgene # 40261) (*91*). Plasmid pRL-CMV was from Promega (#E2261), and pSpCas9(BB)-2A-Puro (PX459) a gift from Feng Zhang (Addgene # 48139) (*118*). Plasmid pGL3-CMV.Luc was a gift from Laurent Guillemot

(University of Geneva). For knocking down Hsf1, oligonucleotides (Table S1) were purchased from Microsynth, annealed, and cloned into pLKO.1 (Addgene #10878). The VSV-G envelope expressing plasmid pMD2.G, and the lentiviral packaging plasmid psPAX2 were gifts from Didier Trono.

Lentiviral particle generation and gene knockdown

5× 10^6 HEK cells in a 10 cm plate were co-transfected with plasmids pLKO.1shHSF1-1 or pLKO.1shHSF1-2 (5 µg), pMD2.G (1.25 µg), and psPAX.2 (3.75 µg) with PEI MAX 40K (Polysciences Inc., # 24765-100) (1:3 DNA to PEI ratio). Suspensions of lentiviral particles were collected and added to the medium of WT and Hsp90α/β KO A549 cells to knock down the expression of Hsf1. Lentiviral control particles were similarly generated and used to express a non-targeting shRNA (not known to target any human mRNA) from plasmid pLKO.1. Transduced cells were selected with 4 µg/ml puromycin (Cayman Chemical # 13884) and used as a pool for further experiments. Knockdowns were validated by immunoblot analyses.

Chronic mild stress models

Heat shock: To induce chronic HS, HEK and its respective Hsp90α/β KO cells, and HCT116 cells were cultured at 39 °C; A549 and its respective Hsp90α/β KO cells, RPE1 cells, and MAFs were cultured at 40 °C. The seeding density was 0.5 - 2× 10^6 cells per 15 cm dish depending on the cell line. Depending on the aim of the experiment, cells were cultured in HS for different time spans as mentioned in the respective figure legends.

Hypoxia: Cells were cultured with 1% O_2 and 5% CO_2 in a 37 °C humidified incubator for a maximum of 4 days. The seeding density was 0.5 - 2× 10^6 cells per 10 cm dish, depending on the cell line. For HEK and its respective Hsp90α/β KO cells, 5 ml fresh medium was added every day to counter the acidification of the culture medium.

Oxidative stress: To generate chronic mild oxidative stress, 5-10 μM sodium arsenite (Ars) was added to the cell culture medium for 4 days.

Proteotoxic stress: For chronic mild proteotoxic stress, 5 μM L-azetidine-2-carboxylic acid (AZC) (Sigma #P8783) was added to the culture medium for 4 days.

Acute oxidative stress model

To generate acute oxidative stress, 2-5 × 10^5 cells were cultured with 25-40 μM sodium arsenite for 1 day.

Measurement of cell size

Cells were detached with trypsin/EDTA (PAN-Biotech #P10-024100), collected in complete medium, and thoroughly washed in Tris-buffered saline (TBS). Single-cell suspensions were resuspended in 100–200 μl (PBS) containing 2.5 µg/ml propidium iodide (PI) (Cayman Chemical #14289-10), for 10 min at room temperature (RT). Cells were analyzed with FACS Gallios flow cytometer (Beckman Coulter), and data were analyzed with the FlowJo software package. Cell populations were gated for size measurements based on the value of the forward scatter (FSC) (fig. S8A). We made the assumption that trypsinized cells are round in shape, and therefore, that the respective FSC values are proportional to the diameter of the cells. The PI-

positive population was excluded from the size measurement analysis. The respective FSC value was converted to a % value. Control experiments showed that initially preparing the cell suspension in medium containing 5% FCS rather than PBS had no impact on the measured values. However, cell size can be changed if cells are in apoptosis. For the experiments where apoptosis could be observed, cells were stained with PI and annexin V (Biolegend #640906) as described below. Cells positive for PI and annexin V were excluded from the size measurement analysis. Again, controls showed that the annexin V buffer had no impact. For all flow cytometric analyses mentioned here or below, a minimum of 10,000 cells were analyzed for each sample.

Cell death assays

PI staining: Cells were stained with PI as mentioned above and then analyzed by flow cytometry.

Annexin V-FITC staining: Following a specific treatment, cells were harvested by trypsinization, washed in phosphate-buffered saline (PBS), and resuspended in 100 μl annexin V-binding buffer (10 mM HEPES pH 7.4, 150 mM NaCl, 2.5 mM $CaCl_2$). 5 μl annexin V-FITC and PI to 2.5 µg /ml were added to the cells and incubated for 15 min at 4 °C.

Cell cycle analyses

Cells were harvested as detailed above. Next, cells were fixed with 70% ice-cold ethanol, washed in PBS, and treated with 100 µg/ml RNase A at RT for 5 min, then

incubated with PI to 50 µg/ml for 15–20 min at RT before flow cytometric analysis. Apoptotic cells were identified by the quantitation of the SubG0 (<2n DNA) cell population (fig. S8B).

Cell proliferation assays

Crystal violet staining: To determine the rate of cell proliferation under chronic HS, 5 × 10^5 cells/well were seeded into 6-well plates and cultured in chronic HS condition as mentioned earlier or at 37 °C. For the heat-adapted cells, they were cultured under chronic HS for 1 week before this assay. One plate was harvested as a control before chronic HS treatment (Day 1). Plates were harvested after 2, 3, and 4 days from seeding. The proliferation of cells was quantitated by crystal violet staining. Briefly, cells were washed with PBS, incubated with 4% formaldehyde in PBS for 20 min, washed again with PBS, then incubated with 0.1% crystal violet solution in distilled water for 30 min. The wells were washed thoroughly with distilled water and air-dried overnight. Crystals were dissolved in glacial acetic acid, and the absorbance was measured at 595 nm with a Cytation 3 Image Reader (Agilent).

Cell counting: To determine the impact of chronic HS on cell proliferation, HEK and A549 cells were seeded at a density of 3–5 × 10^6 cells per 20 ml in a 15 cm plate and subjected to mild HS at 39 °C and 40 °C for HEK and A549 cells, respectively. A parallel set was maintained at 37 °C as control. Every 7 days, cells were harvested by trypsinization and counted using a hemocytometer under the light microscope with the trypan blue exclusion assay.

Phase contrast and fluorescence microscopy

Cellular morphology and cell culture density were analyzed using an inverted light microscope (Olympus CK2), and phase contrast images were captured with a Dino-lite camera using the software DinoXcope. To visualize the impact of chronic HS on the actin network, cells were grown under chronic HS conditions on a poly-L-lysine-coated coverslip for 4 days, before being washed with PBS and fixed with 3% glyoxal solution (*119*). Actin was stained with Phalloidin-Alexa488 (Thermo Fisher Scientific #A12379), and the nucleus was stained with diamidino-2-phenylindole dye (DAPI) (1:30,000 in PBS, from 1 mg/ml stock solution (Thermo Fisher Scientific #62248)). Coverslips were mounted on glass slides using Mowiol. Cells were visualized, and images were captured with a fluorescence microscope (Zeiss, Germany).

Hsf1 activity assay

To check the Hsf1 activity at 37 °C, under chronic HS, and upon capsaicin treatment, at first, 4×10^4 cells per 400 μl were seeded in 24-well plates. Cells were co-transfected with the Hsf1 luciferase reporter plasmid HSE (WT)-Luc and the Renilla luciferase internal transfection control (plasmid pRL-CMV). 24h after transfection, cells were cultured under chronic HS conditions for 2 days or in capsaicin (10-250 μM) for 4 days. Then, cells were lysed, and firefly and Renilla luciferase activities were measured using the Dual-Luciferase detection kit (Promega #E1910) with a bioluminescence plate reader (Citation, BioTek). Firefly luciferase activities were normalized to those of Renilla luciferase. The corresponding fold change of Hsf1 activity under chronic HS was normalized to their respective Hsf1 activity at 37 °C. In experiments where Hsf1 activity was measured after overexpressing WT or mutant

Hsf1, HSE (WT)-Luc and pRL-CMV were co-transfected with the respective expression plasmids.

FRAP experiments

FRAP experiments were carried out on a Leica SP8 confocal microscope using a 63x oil immersion objective. For *in vivo* measurements of cytoplasmic density, cells were transiently transfected with EGFP expression plasmid pEGFP-C1. Fluorescence was bleached within a circular area of 10 μm^2 with homogeneous fluorescence within the cytoplasm and a background zone outside the cell. After bleaching, images were taken every 1.29 seconds for HEK and its corresponding Hsp90α/β KO cells and 0.22 seconds for A549 and its corresponding Hsp90α/β KO cells for a total of 30 images. The data were used for the calculation of t-half and diffusion coefficients by a one-phase exponential association function, and recovery curves were built using GraphPad Prism 8 (GraphPad Software, Inc., La Jolla, CA).

Protein extraction and analysis

Quantification of cellular protein: To quantify the amount of total soluble protein per cell, 5 x 10^6 cells per experimental condition were harvested, pellets were washed at least twice with PBS, and then lysed in ice-cold lysis buffer (20 mM Tris-HCl pH 7.4, 2 mM EDTA, 150 mM NaCl, 1.2% sodium deoxycholate, 1.2% Triton X-100, protease inhibitor cocktail (Thermo Fisher Scientific #78429), and phosphatase inhibitor cocktail (Thermo Fisher Scientific #78420)). Cell lysates were sonicated for 15 min at high power with the Bioruptor sonicator (Diagenode). Protein quantification was performed using the Bradford reagent (Biorad #5000001), measuring absorbance at

595 nm. To visualize the amount of total protein in each experimental condition, the same volume of cell lysates was mixed with SDS sample buffer and run on 10% SDS-PAGE, and proteins were stained with Coomassie blue for 1 h and de-stained overnight in water.

Analysis of cell size to total protein ratio: Cells from different experimental conditions were fixed for 10 min in 4% formaldehyde, washed with PBS, and permeabilized in 100% methanol for 10 min at -20 °C. Methanol was removed, and cells were washed once with 0.2 M sodium bicarbonate, followed by staining in 0.5 ml 0.2 M sodium bicarbonate containing 50 mg/ml Alexa Fluor 488 NHS Ester (succinimidyl ester) (Thermo Fisher Scientific #A20100) for 30 min at RT. Cells were then analyzed using flow cytometry. The amount of protein per cell was quantitated as log of the mean fluorescent intensity (MFI) values (detected in the FL1 channel, i.e. MFI-FL1). Relative cell size was deduced from the FSC values (see above).

Assay of protein translation: To measure *de novo* protein translation, cells were seeded at a density of 1.2–1.5 × 10^6 per 10 ml in a 10 cm plate. Cells were then treated with 1 µM puromycin for 0–2.5 h, while being cultured at 37 °C or 39 °C. Cells were harvested and lysed in lysis buffer (20 mM Tris-HCl pH 7.4, 2 mM EDTA, 150 mM NaCl, 1.2% sodium deoxycholate, 1.2% Triton-X100, 200 mM iodoacetamide, protease inhibitor cocktail). 75 µg of clarified cell lysates were separated by 10% SDS-PAGE and immunoblotted for newly synthesized proteins or polypeptides with anti-puromycin antibodies. The intensities of the corresponding lanes reflect the total amount of global protein translation for that time point. To

determine *de novo* protein translation at the single cell level in relation to cell size, cells were maintained at 39 °C for 4 h, 1 day, and 4 days. Nascent polypeptides were labelled using Click-iT Plus OPP Alexa Fluor 594 (Thermo Fisher Scientific #C10457) as described in the manufacturer's protocol. Briefly, O-propargyl-puromycin (OPP) (2 µM) was added to cultured cells up to 4 h after the above-mentioned incubation at 39 °C. In parallel, a control set was done at 37 °C. Cells were then washed with PBS, fixed in 3.7% formaldehyde in PBS, permeabilized in 0.5% Triton X-100 in PBS, and incubated at RT for 15 min. The permeabilization buffer was washed off with PBS. Click-iT Plus OPP reaction cocktail was added and incubated for 30 min at RT, protected from light. The reaction cocktail was removed and washed once with 1 ml of Click-iT Reaction Rinse Buffer, further washed with PBS, and kept in PBS until newly synthesized proteins were quantitated using flow cytometry (fig. S9) and expressed as log MFI values, and relative to cell size.

Immunoblot analyses: Lysates of cells (20–100 µg) were subjected to SDS-PAGE and transferred onto a nitrocellulose membrane (GVS Life Science) with a wet blot transfer system (VWR #BTV100). Membranes were blocked with 2–5% non-fat dry milk or bovine serum albumin in TBS with 0.2% Tween 20 (TBST) and incubated with primary antibodies overnight at 4°C. Then they were washed with TBST, incubated with the corresponding secondary antibodies for 1 h at RT, and developed using the WesternBright chemiluminescent substrate (Advansta #K-12045-D50). Images were captured using a LI-COR Odyssey or Amersham ImageQuant 800 image recorder. The EZ-Run Prestained Protein Ladder (Thermo Fisher Scientific) or the AcuteBand

Prestained Protein ladder (Lubioscience) were used as protein molecular weight markers. Details of primary and secondary antibodies are given in Table S2.

Autophagic flux measurement

Cells seeded in 6-well plate at a density of 4×10^5 per 2 ml were transfected with the autophagy reporter plasmid FUW mCherry-GFP-LC3 as described above. 24 h after transfection, cells were subjected to chronic HS for 2 days. Cells were harvested by trypsinization, and GFP- and mCherry-positive cells were measured by flow cytometry (fig. S10A). The autophagic flux was measured by calculating the ratio of the MFI of mCherry and GFP-positive cells. A higher relative ratio of mCherry/GFP is indicative of a higher autophagic flux.

***In vivo* UPS activity assay**

Cells seeded at a density of 5×10^5 per 2 ml in 6-well plates were transfected with plasmids Ub-M-GFP and Ub-R-GFP for expression of stable and degradation-prone GFP, respectively (*89*). The next day, the medium was changed, and cells were cultured at 37 °C or 39 °C for 2 days. Cells were then harvested by trypsinization and GFP-positive cells were quantitated by flow cytometry. The *in vivo* UPS activity was expressed as the MFI of Ub-M-GFP-positive cells minus the MFI of Ub-R-GFP-positive cells (fig. S10B). Fold change of UPS activity in HS was normalized to the corresponding activity at 37 °C. Fold change of UPS activity of Hsp90α/β KO cells was also normalized to the fold change relative to WT cells.

***In vivo* luciferase refolding assay**

Cells cultured at 37 °C or cells adapted at 39 °C for 2 days were transfected with the luciferase expression vector pGL3-CMV.Luc. Cells were subjected to an acute HS at 43 °C for 15 min to denature luciferase, followed by incubation at 37 °C for the control cells or at 39 °C for the heat-adapted cell for 1–3 h to allow refolding of luciferase. Cells were harvested by centrifugation and lysed with the Passive Lysis Buffer of the Dual-Luciferase detection kit (Promega). 10 μl cell extract was mixed with an equal volume of firefly luciferase assay substrate from the kit, and the luciferase luminescence signals were measured with a bioluminescence plate reader (Citation, BioTek).

In vitro proteasomal activity assay

Cells cultured at 37 °C or at 39 °C were harvested and washed. Cell pellets were resuspended in lysis buffer (25 mM Tris-HCl pH 7.4, 250 mM sucrose, 5 mM $MgCl_2$, 1% IGEPAL, 1 mM DTT, 1 mM ATP) and incubated for 10–15 min on ice. Samples were centrifuged at 16,100 × g for 20 min, and supernatants were collected for the proteasomal activity assay. Equal amounts of protein (50 μg) for each sample were diluted in proteasomal reaction buffer (50 mM Tris-HCl pH 7.4, 5 mM $MgCl_2$, 1 mM DTT, 1 mM ATP) in a 96-well opaque bottom white plate and 50 μM N-succinyl-Leu-Leu-Val-Tyr-7-amino-4-methyl-coumarin (suc-LLVY-AMC) (Enzo Life Sciences, #BML-P802-0005) was added to each well. AMC fluorescence was measured at 460 nm for 5–60 min, with an excitation at 380 nm. All fluorescence measurements were recorded using a plate reader (Cytation 3, BioTek).

Protein aggregation

To analyze polyglutamine (polyQ) protein aggregation within cells, cells were seeded on glass coverslips and transfected with the plasmid pEGFP-Q74 and 24 h after transfection, cells were placed at 39 °C and the respective controls at 37 °C. 42 h after transfection, cells were fixed with 4% paraformaldehyde and mounted on glass slides using Mowiol. EGFP-positive cells were visualized, and images were captured with a fluorescence microscope (Zeiss, Germany).

Increase and reduction of cell size with various inhibitors

To increase the cell size, 2×10^5 cells in 3 ml were seeded in 6-well plates and treated with the Cdk4/6 inhibitor abemaciclib (MedChemExpress, #HY-16297A-5MG) at 50-100 nM for 2-3 days. At this point, one experimental set was harvested. To reduce the cell size, 2×10^5 cells in 3 ml were seeded in 6-well plates, and treated with 5-10 nM rapamycin (Sigma-Aldrich, #553210), or 100 ng/ml cycloheximide (CHX) for 2-3 days. Alternatively, cell size was reduced by replacing the standard growth medium 24 h after seeding with medium containing only 1% FBS. Parallel sets that were not harvested were washed with fresh medium and subjected to other stress treatments. Cell size and cell death were determined by flow cytometry as described above.

Proteomic analyses

Protein digestion: HEK WT and their respective Hsp90α/β KO cells were cultured at 37 °C, and at 39 °C for 1 day and 4 days. Cells were harvested and snap-frozen. Replicate samples were digested according to a modified version of the iST method (named miST method) (*120*). Briefly, frozen cell pellets were resuspended in 3 ml miST lysis buffer (1% sodium deoxycholate, 100 mM Tris pH 8.6, 10 mM DTT).

Resuspended samples were sonicated and heated at 95 °C for 5 min. After quantification with tryptophan fluorescence, 100 µg of samples in 50 µl buffer were diluted 1:1 (v:v) with water. Reduced disulfides were alkylated by adding ¼ volume of 160 mM chloroacetamide (final 32 mM) and incubating at 25 °C for 45 min in the dark. Samples were adjusted to 3 mM EDTA and digested with 1.0 µg Trypsin/LysC mix (Promega #V5073) for 1 h at 37 °C, followed by a second 1-h digestion with a second aliquot of 0.5 µg trypsin. To remove sodium deoxycholate, two sample volumes of isopropanol containing 1% trifluoroacetic acid (TFA) were added to the digests, and the samples were desalted on a strong cation exchange (SCX) plate (Oasis MCX; Waters Corp., Milford, MA) by centrifugation. After washing with isopropanol/1% TFA, peptides were eluted in 200 µl of 80% acetonitrile, 19% water, 1% (v/v) NH_3.

Peptide fractionation for library construction: After redissolution of samples in 1.0 ml of loading buffer (2% acetonitrile with 0.05% TFA), aliquots (10 µl) of samples were pooled and separated into 6 fractions by off-line basic reversed-phase (bRP) using the Pierce High pH Reversed-Phase Peptide Fractionation Kit (Thermo Fisher Scientific). The fractions were collected in 7.5, 10, 12.5, 15, 17.5, and 50% acetonitrile in 0.1% triethylamine (~pH 10). Dried bRP fractions were redissolved in 40 µl loading buffer, and 4 µl were injected for LC-MS/MS analyses.

LC-MS/MS: LC-MS/MS analyses were carried out on a TIMS-TOF Pro (Bruker, Bremen, Germany) mass spectrometer interfaced through a nanospray ion source ("captive spray") to an Ultimate 3000 RSLCnano HPLC system (Dionex). Peptides

were separated on a reversed-phase custom-packed 40 cm C18 column (75 µm ID, 100 Å, Reprosil Pur 1.9 μm particles, Dr. Maisch, Germany) at a flow rate of 0.250 µl /min with a 2-27% acetonitrile gradient in 93 min followed by a ramp to 45% in 15 min and to 90% in 5 min (all solvents contained 0.1% formic acid). Identical LC gradients were used for DDA and DIA measurements.

Library creation: Raw Bruker MS data were processed directly with Spectronaut 15.4 (Biognosys, Schlieren, Switzerland). A library was constructed from the DDA bRP fraction data by searching the reference human proteome (www.uniprot.org; accessed on September 3rd, 2020, containing 75,796 sequences). For identification, peptides of 7-52 AA length were considered, cleaved with trypsin/P specificity, and a maximum of 2 missed cleavages. Carbamidomethylation of cysteine (fixed), methionine oxidation and N-terminal protein acetylation (variable) were the modifications applied. Mass calibration was dynamic and based on a first database search. The Pulsar engine was used for peptide identification. Protein inference was performed with the IDPicker algorithm. Spectra, peptide and protein identifications were all filtered at 1% FDR against a decoy database. Specific filtering for library construction removed fragments corresponding to less than 3 AA and fragments outside the 300-1800 m/z range. Also, only fragments with a minimum base peak intensity of 5% were kept. Precursors with less than 3 fragments were also eliminated, and only the best 6 fragments were kept per precursor. No filtering was done on the basis of charge state, and a maximum of 2 missed cleavages was allowed. Shared (non-proteotypic) peptides were kept. The library created contained 119,573 precursors mapping to 91,154 stripped sequences, of which 35,119 were

proteotypic. These corresponded to 8,632 protein groups (12,252 proteins). Of these, 959 were single hits (one peptide precursor). In total 701,091 fragments were used for quantitation.

DIA quantitation: Peptide-centric analysis of DIA data was done with Spectronaut 15.4 using the library described above. Single hits proteins (defined as matched by one stripped sequence only) were kept in the Spectronaut analysis. Peptide quantitation was based on XIC area, for which a minimum of 1 and a maximum of 3 (the 3 best) precursors were considered for each peptide, from which the median value was selected. Quantities for protein groups were derived from inter-run peptide ratios based on MaxLFQ algorithm (Cox et al 2014). Global normalization of runs/samples was done based on the median of peptides.

Data processing and statistical tests: All subsequent analyses were done with the Perseus software package (version 1.6.15.0). Intensity values were log2-transformed, and after assignment to groups, t-tests were carried out with permutation-based FDR correction for multiple testing (Q-value threshold <0.01). The difference of means obtained from the tests was used for 1D enrichment analysis on associated GO/KEGG annotations as described (Cox and Mann, 2012). The enrichment analysis was also FDR-filtered (Benjamini-Hochberg, Q-val<0.02). The data of the proteomic analysis are supplied as data S1.

Ribosome and polysome fractionation

Polysome fractionation was performed at the “BioCode: RNA to Proteins” core facility of the Faculty of Medicine of the University of Geneva. Cells were cultured at 37 °C or 39 °C for 4 days. Before harvesting the cells, 100 μg/ml CHX was added to the medium, and cells were maintained in the respective incubator for 15-20 min. Cells were then harvested and washed in ice-cold PBS containing 100 μg/ml CHX, snap-frozen and proceeded to the next steps. Cells were weighed, and resuspended in lysis buffer (50 mM Tris-HCl pH 7.4, 100 mM KCl, 1.5 mM $MgCl_2$, 1.5% Triton X-100, 1 mM DTT, 100 μg/ml CHX, 1 mg/ml heparin, 25 u/ml Turbo DNase I (Roche, #04716728001), 25 u/μl SUPERaseIn RNase inhibitor (Invitrogen, #AM2694), protease inhibitors (Roche, #04693132001)) at 200 μl lysis buffer per 100 μg pellet. Cell suspensions were passed through a 25G needle 10-12 times. Cell debris were pelleted at 20,000 g at 4 °C for 20 min. The total RNA concentration of the supernatant was determined. Cell lysates containing 350 μg of total RNA were loaded onto linear 20-60% sucrose gradients prepared with the gradient buffer (50 mM Tris-HCl pH 7.4, 100 mM KCl, 1.5 mM $MgCl_2$, 1 mM DTT, 100 μg/ml CHX). Ribosomes/polysomes were centrifuged at 247,600 g (38,000 rpm) in a SW41 Ti rotor (Beckman Coulter, #331362) for 3 h 30 min at 4 °C. Fractionated ribosomes/polysomes were measured and collected using a density gradient fractionation system (ISCO).

General data analyses

Data processing and analyses were performed using GraphPad Prism (version 8).

References

1. D. Kultz, Evolution of cellular stress response mechanisms. *J. Exp. Zool. A Ecol. Integr. Physiol.* **333**, 359-378 (2020).
2. T. N. Kristensen, T. Ketola, I. Kronholm, Adaptation to environmental stress at different timescales. *Ann. N. Y. Acad. Sci.* **1476**, 5-22 (2020).
3. R. Bijlsma, V. Loeschcke, Environmental stress, adaptation and evolution: an overview. *J. Evol. Biol.* **18**, 744-749 (2005).
4. D. Kultz, Defining biological stress and stress responses based on principles of physics. *J. Exp. Zool. A Ecol. Integr. Physiol.* **333**, 350-358 (2020).
5. N. M. Rzechorzek, M. J. Thrippleton, F. M. Chappell, G. Mair, A. Ercole, M. Cabeleira, C.-T. H. R. I. S.-S. Participants, Investigators, J. Rhodes, I. Marshall, J. S. O'Neill, A daily temperature rhythm in the human brain predicts survival after brain injury. *Brain* **145**, 2031-2048 (2022).
6. S. S. Evans, E. A. Repasky, D. T. Fisher, Fever and the thermal regulation of immunity: the immune system feels the heat. *Nat. Rev. Immunol.* **15**, 335-349 (2015).
7. D. van Norren, J. J. Vos, Light damage to the retina: an historical approach. *Eye* **30**, 169-172 (2016).
8. F. C. Baker, F. Siboza, A. Fuller, Temperature regulation in women: Effects of the menstrual cycle. *Temperature* **7**, 226-262 (2020).
9. M. A. Mainster, T. J. White, J. H. Tips, P. W. Wilson, Retinal-temperature increases produced by intense light sources. *J. Opt. Soc. Am.* **60**, 264-270 (1970).

10. B. Taborsky, S. English, T. W. Fawcett, B. Kuijper, O. Leimar, J. M. McNamara, S. Ruuskanen, C. Sandi, Towards an evolutionary theory of stress responses. *Trends Ecol. Evol.* **36**, 39-48 (2021).

11. X. D. Liu, P. C. Liu, N. Santoro, D. J. Thiele, Conservation of a stress response: human heat shock transcription factors functionally substitute for yeast HSF. *EMBO J.* **16**, 6466-6477 (1997).

12. J. Li, J. Labbadia, R. I. Morimoto, Rethinking HSF1 in stress, development, and organismal health. *Trends Cell Biol.* **27**, 895-905 (2017).

13. K. Richter, M. Haslbeck, J. Buchner, The heat shock response: life on the verge of death. *Mol. Cell* **40**, 253-266 (2010).

14. A. Vihervaara, L. Sistonen, HSF1 at a glance. *J. Cell Sci.* **127**, 261-266 (2014).

15. S. Lindquist, E. A. Craig, The heat-shock proteins. *Annu. Rev. Genet.* **22**, 631-677 (1988).

16. F. U. Hartl, A. Bracher, M. Hayer-Hartl, Molecular chaperones in protein folding and proteostasis. *Nature* **475**, 324-332 (2011).

17. L. B. Persson, V. S. Ambati, O. Brandman, Cellular control of viscosity counters changes in temperature and energy availability. *Cell* **183**, 1572-1585 (2020).

18. D. Balchin, M. Hayer-Hartl, F. U. Hartl, In vivo aspects of protein folding and quality control. *Science* **353**, aac4354 (2016).

19. J. L. Johnson, Evolution and function of diverse Hsp90 homologs and cochaperone proteins. *Biochim. Biophys. Acta* **1823**, 607-613 (2012).

20. M. Taipale, D. F. Jarosz, S. Lindquist, HSP90 at the hub of protein homeostasis: emerging mechanistic insights. *Nat. Rev. Mol. Cell. Biol.* **11**, 515-528 (2010).

21. K. Bhattacharya, D. Picard, The Hsp70-Hsp90 go-between Hop/Stip1/Sti1 is a proteostatic switch and may be a drug target in cancer and neurodegeneration. *Cell. Mol. Life Sci.* **78**, 7257-7273 (2021).

22. K. Bhattacharya, L. Weidenauer, T. M. Luengo, E. C. Pieters, P. C. Echeverria, L. Bernasconi, D. Wider, Y. Sadian, M. B. Koopman, M. Villemin, C. Bauer, S. G. D. Rüdiger, M. Quadroni, D. Picard, The Hsp70-Hsp90 co-chaperone Hop/Stip1 shifts the proteostatic balance from folding towards degradation. *Nat. Commun.* **11**, 5975 (2020).

23. P. C. Echeverria, A. Bernthaler, P. Dupuis, B. Mayer, D. Picard, An interaction network predicted from public data as a discovery tool: application to the Hsp90 molecular chaperone machine. *PLoS ONE* **6**, e26044 (2011).

24. I. Fierro-Monti, P. Echeverria, J. Racle, C. Hernandez, D. Picard, M. Quadroni, Dynamic impacts of the inhibition of the molecular chaperone Hsp90 on the T-cell proteome have implications for anti-cancer therapy. *PLoS ONE* **8**, e80425 (2013).

25. E. A. Nollen, R. I. Morimoto, Chaperoning signaling pathways: molecular chaperones as stress-sensing 'heat shock' proteins. *J. Cell Sci.* **115**, 2809-2816 (2002).

26. M. Mollapour, S. Tsutsumi, L. Neckers, Hsp90 phosphorylation, Wee1 and the cell cycle. *Cell Cycle* **9**, 2310-2316 (2010).

27. A. Finka, P. Goloubinoff, Proteomic data from human cell cultures refine mechanisms of chaperone-mediated protein homeostasis. *Cell Stress Chaperones* **18**, 591-605 (2013).

28. K. Bhattacharya, S. Maiti, S. Zahoran, L. Weidenauer, D. Hany, D. Wider, L. Bernasconi, M. Quadroni, M. Collart, D. Picard, Translational reprogramming in response to accumulating stressors ensures critical threshold levels of Hsp90 for mammalian life. *Nat. Commun.* **13**, 6271 (2022).

29. A. S. Sreedhar, E. Kalmar, P. Csermely, Y. F. Shen, Hsp90 isoforms: functions, expression and clinical importance. *FEBS Lett.* **562**, 11-15 (2004).

30. S. Maiti, D. Picard, Cytosolic Hsp90 isoform-specific functions and clinical significance. *Biomolecules* **12**, 1166 (2022).

31. J. Labbadia, R. I. Morimoto, The biology of proteostasis in aging and disease. *Annu. Rev. Biochem.* **84**, 435-464 (2015).

32. M. S. Hipp, P. Kasturi, F. U. Hartl, The proteostasis network and its decline in ageing. *Nat. Rev. Mol. Cell. Biol.* **20**, 421-435 (2019).

33. D. Vilchez, I. Saez, A. Dillin, The role of protein clearance mechanisms in organismal ageing and age-related diseases. *Nat. Commun.* **5**, 5659 (2014).

34. Y. Lu, B. Brommer, X. Tian, A. Krishnan, M. Meer, C. Wang, D. L. Vera, Q. Zeng, D. Yu, M. S. Bonkowski, J. H. Yang, S. Zhou, E. M. Hoffmann, M. M. Karg, M. B. Schultz, A. E. Kane, N. Davidsohn, E. Korobkina, K. Chwalek, L. A. Rajman, G. M. Church, K. Hochedlinger, V. N. Gladyshev, S. Horvath, M. E. Levine, M. S. Gregory-Ksander, B. R. Ksander, Z. He, D. A. Sinclair, Reprogramming to recover youthful epigenetic information and restore vision. *Nature* **588**, 124-129 (2020).

35. N. Kourtis, N. Tavernarakis, Cellular stress response pathways and ageing: intricate molecular relationships. *EMBO J.* **30**, 2520-2531 (2011).

36. B. G. Childs, M. Durik, D. J. Baker, J. M. van Deursen, Cellular senescence in aging and age-related disease: from mechanisms to therapy. *Nat. Med.* **21**, 1424-1435 (2015).

37. D. McHugh, J. Gil, Senescence and aging: Causes, consequences, and therapeutic avenues. *J. Cell Biol.* **217**, 65-77 (2018).

38. A. Calcinotto, J. Kohli, E. Zagato, L. Pellegrini, M. Demaria, A. Alimonti, Cellular senescence: aging, cancer, and injury. *Physiol. Rev.* **99**, 1047-1078 (2019).

39. J. Yang, H. Dungrawala, H. Hua, A. Manukyan, L. Abraham, W. Lane, H. Mead, J. Wright, B. L. Schneider, Cell size and growth rate are major determinants of replicative lifespan. *Cell Cycle* **10**, 144-155 (2011).

40. Y. Mitsui, E. L. Schneider, Relationship between cell replication and volume in senescent human diploid fibroblasts. *Mech. Ageing Dev.* **5**, 45-56 (1976).

41. L. Hayflick, P. S. Moorhead, The serial cultivation of human diploid cell strains. *Exp. Cell Res.* **25**, 585-621 (1961).

42. M. Adolphe, X. Ronot, P. Jaffray, C. Hecquet, J. Fontagne, P. Lechat, Effects of donor's age on growth kinetics of rabbit articular chondrocytes in culture. *Mech. Ageing Dev.* **23**, 191-198 (1983).

43. T. Mammoto, Y. S. Torisawa, M. Muyleart, K. Hendee, C. Anugwom, D. Gutterman, A. Mammoto, Effects of age-dependent changes in cell size on endothelial cell proliferation and senescence through YAP1. *Aging* **11**, 7051-7069 (2019).

44. Z. N. Demidenko, M. V. Blagosklonny, Growth stimulation leads to cellular senescence when the cell cycle is blocked. *Cell Cycle* **7**, 3355-3361 (2008).

45. V. J. Cristofalo, D. Kritchevsky, Cell size and nucleic acid content in the diploid human cell line WI-38 during aging. *Med. Exp. Int. J. Exp. Med.* **19**, 313-320 (1969).

46. J. A. Treton, Y. Courtois, Evolution of the distribution, proliferation and ultraviolet repair capacity of rat lens epithelial cells as a function of maturation and aging. *Mech. Ageing Dev.* **15**, 251-267 (1981).

47. G. E. Neurohr, R. L. Terry, J. Lengefeld, M. Bonney, G. P. Brittingham, F. Moretto, T. P. Miettinen, L. P. Vaites, L. M. Soares, J. A. Paulo, J. W. Harper, S. Buratowski, S. Manalis, F. J. van Werven, L. J. Holt, A. Amon, Excessive cell growth causes cytoplasm dilution and contributes to senescence. *Cell* **176**, 1083-1097 (2019).

48. M. C. Lanz, E. Zatulovskiy, M. P. Swaffer, L. Zhang, I. Ilerten, S. Zhang, D. S. You, G. Marinov, P. McAlpine, J. E. Elias, J. M. Skotheim, Increasing cell size remodels the proteome and promotes senescence. *Mol. Cell* **82**, 3255-3269 (2022).

49. C. Boehlke, F. Kotsis, V. Patel, S. Braeg, H. Voelker, S. Bredt, T. Beyer, H. Janusch, C. Hamann, M. Godel, K. Muller, M. Herbst, M. Hornung, M. Doerken, M. Kottgen, R. Nitschke, P. Igarashi, G. Walz, E. W. Kuehn, Primary cilia regulate mTORC1 activity and cell size through Lkb1. *Nat. Cell Biol.* **12**, 1115-1122 (2010).

50. S. Dhawan, S. Georgia, A. Bhushan, Formation and regeneration of the endocrine pancreas. *Curr. Opin. Cell Biol.* **19**, 634-645 (2007).

51. A. P. Hall, C. R. Elcombe, J. R. Foster, T. Harada, W. Kaufmann, A. Knippel, K. Kuttler, D. E. Malarkey, R. R. Maronpot, A. Nishikawa, T. Nolte, A. Schulte, V. Strauss, M. J. York, Liver hypertrophy: a review of adaptive (adverse and non-adverse) changes--conclusions from the 3rd International ESTP expert workshop. *Toxicol. Pathol.* **40**, 971-994 (2012).

52. M. Samak, J. Fatullayev, A. Sabashnikov, M. Zeriouh, B. Schmack, M. Farag, A. F. Popov, P. M. Dohmen, Y. H. Choi, T. Wahlers, A. Weymann, Cardiac hypertrophy: an introduction to molecular and cellular basis. *Med. Sci. Monit. Basic Res.* **22**, 75-79 (2016).

53. M. B. Ginzberg, R. Kafri, M. Kirschner, Cell biology. On being the right (cell) size. *Science* **348**, 1245075 (2015).

54. G. N. Somero, The cellular stress response and temperature: Function, regulation, and evolution. *J. Exp. Zool .A Ecol. Integr. Physiol.* **333**, 379-397 (2020).

55. A. Tzur, J. K. Moore, P. Jorgensen, H. M. Shapiro, M. W. Kirschner, Optimizing optical flow cytometry for cell volume-based sorting and analysis. *PLoS ONE* **6**, e16053 (2011).

56. G. Varsano, Y. Wang, M. Wu, Probing mammalian cell size homeostasis by channel-assisted cell reshaping. *Cell Rep.* **20**, 397-410 (2017).

57. C. Cadart, S. Monnier, J. Grilli, P. J. Saez, N. Srivastava, R. Attia, E. Terriac, B. Baum, M. Cosentino-Lagomarsino, M. Piel, Size control in mammalian cells involves modulation of both growth rate and cell cycle duration. *Nat. Commun.* **9**, 3275 (2018).

58. T. P. Miettinen, M. J. Caldez, P. Kaldis, M. Björklund, Cell size control - a mechanism for maintaining fitness and function. *Bioessays* **39** (2017).

59. A. L. Horwich, Molecular chaperones in cellular protein folding: the birth of a field. *Cell* **157**, 285-288 (2014).

60. U. Jakob, J. Buchner, Assisting spontaneity: the role of Hsp90 and small Hsps as molecular chaperones. *Trends Biochem. Sci.* **19**, 205-211 (1994).

61. M. P. Mayer, B. Bukau, Molecular chaperones: the busy life of Hsp90. *Curr. Biol.* **9**, R322-325 (1999).

62. J. C. Young, I. Moarefi, F. U. Hartl, Hsp90: a specialized but essential protein-folding tool. *J. Cell Biol.* **154**, 267-273 (2001).

63. D. Picard, Heat-shock protein 90, a chaperone for folding and regulation. *Cell. Mol. Life Sci.* **59**, 1640-1648 (2002).

64. S. Tamura, T. Marunouchi, K. Tanonaka, Heat-shock protein 90 modulates cardiac ventricular hypertrophy via activation of MAPK pathway. *J. Mol. Cell. Cardiol.* **127**, 134-142 (2019).

65. J. Anckar, L. Sistonen, Regulation of HSF1 function in the heat stress response: implications in aging and disease. *Annu. Rev. Biochem.* **80**, 1089-1115 (2011).

66. R. Gomez-Pastor, E. T. Burchfiel, D. J. Thiele, Regulation of heat shock transcription factors and their roles in physiology and disease. *Nat. Rev. Mol. Cell. Biol.* **19**, 4-19 (2018).

67. M. D. Leach, S. Budge, L. Walker, C. Munro, L. E. Cowen, A. J. Brown, Hsp90 orchestrates transcriptional regulation by Hsf1 and cell wall

remodelling by MAPK signalling during thermal adaptation in a pathogenic yeast. *PLoS Pathog.* **8**, e1003069 (2012).

68. J. Zou, Y. Guo, T. Guettouche, D. F. Smith, R. Voellmy, Repression of heat shock transcription factor HSF1 activation by HSP90 (HSP90 complex) that forms a stress-sensitive complex with HSF1. *Cell* **94**, 471-480 (1998).

69. J. H. Lee, J. Gao, P. A. Kosinski, S. J. Elliman, T. E. Hughes, J. Gromada, D. M. Kemp, Heat shock protein 90 (HSP90) inhibitors activate the heat shock factor 1 (HSF1) stress response pathway and improve glucose regulation in diabetic mice. *Biochem. Biophys. Res. Commun.* **430**, 1109-1113 (2013).

70. N. Hentze, L. Le Breton, J. Wiesner, G. Kempf, M. P. Mayer, Molecular mechanism of thermosensory function of human heat shock transcription factor Hsf1. *eLife* **5**, e11576 (2016).

71. T. Kijima, T. L. Prince, M. L. Tigue, K. H. Yim, H. Schwartz, K. Beebe, S. Lee, M. A. Budzynski, H. Williams, J. B. Trepel, L. Sistonen, S. Calderwood, L. Neckers, HSP90 inhibitors disrupt a transient HSP90-HSF1 interaction and identify a noncanonical model of HSP90-mediated HSF1 regulation. *Sci. Rep.* **8**, 6976 (2018).

72. T. Hagenacker, F. Splettstoesser, W. Greffrath, R. D. Treede, D. Busselberg, Capsaicin differentially modulates voltage-activated calcium channel currents in dorsal root ganglion neurones of rats. *Brain Res.* **1062**, 74-85 (2005).

73. Z. Bromberg, P. Goloubinoff, Y. Saidi, Y. G. Weiss, The membrane-associated transient receptor potential vanilloid channel is the central heat shock receptor controlling the cellular heat shock response in epithelial cells. *PLoS ONE* **8**, e57149 (2013).

74. S. Joshi, T. Wang, T. L. S. Araujo, S. Sharma, J. L. Brodsky, G. Chiosis, Adapting to stress - chaperome networks in cancer. *Nat. Rev. Cancer* **18**, 562-575 (2018).

75. P. Yan, T. Wang, M. L. Guzman, R. I. Peter, G. Chiosis, Chaperome networks - redundancy and implications for cancer treatment. *Adv. Exp. Med. Biol.* **1243**, 87-99 (2020).

76. D. F. Berenson, E. Zatulovskiy, S. Xie, J. M. Skotheim, Constitutive expression of a fluorescent protein reports the size of live human cells. *Mol. Biol. Cell* **30**, 2985-2995 (2019).

77. H. Kempe, A. Schwabe, F. Cremazy, P. J. Verschure, F. J. Bruggeman, The volumes and transcript counts of single cells reveal concentration homeostasis and capture biological noise. *Mol. Biol. Cell* **26**, 797-804 (2015).

78. J. Lin, A. Amir, Homeostasis of protein and mRNA concentrations in growing cells. *Nat. Commun.* **9**, 4496 (2018).

79. R. Jobava, Y. Mao, B. J. Guan, D. Hu, D. Krokowski, C. W. Chen, X. E. Shu, E. Chukwurah, J. Wu, Z. Gao, L. L. Zagore, W. C. Merrick, A. Trifunovic, A. C. Hsieh, S. Valadkhan, Y. Zhang, X. Qi, E. Jankowsky, I. Topisirovic, D. D. Licatalosi, S. B. Qian, M. Hatzoglou, Adaptive translational pausing is a hallmark of the cellular response to severe environmental stress. *Mol. Cell* **81**, 4191-4208 (2021).

80. R. Shalgi, J. A. Hurt, I. Krykbaeva, M. Taipale, S. Lindquist, C. B. Burge, Widespread regulation of translation by elongation pausing in heat shock. *Mol. Cell* **49**, 439-452 (2013).

81. V. M. Advani, P. Ivanov, Translational control under stress: reshaping the translatome. *Bioessays* **41**, e1900009 (2019).

82. B. Liu, Y. Han, S. B. Qian, Cotranslational response to proteotoxic stress by elongation pausing of ribosomes. *Mol. Cell* **49**, 453-463 (2013).

83. R. C. Wek, Role of eIF2α kinases in translational control and adaptation to cellular stress. *Cold Spring Harb. Perspect. Biol.* **10**, a032870 (2018).

84. K. Pakos-Zebrucka, I. Koryga, K. Mnich, M. Ljujic, A. Samali, A. M. Gorman, The integrated stress response. *EMBO Rep.* **17**, 1374-1395 (2016).

85. D. C. Fingar, S. Salama, C. Tsou, E. Harlow, J. Blenis, Mammalian cell size is controlled by mTOR and its downstream targets S6K1 and 4EBP1/eIF4E. *Genes Dev.* **16**, 1472-1487 (2002).

86. K. H. Su, J. Cao, Z. Tang, S. Dai, Y. He, S. B. Sampson, I. J. Benjamin, C. Dai, HSF1 critically attunes proteotoxic stress sensing by mTORC1 to combat stress and promote growth. *Nat. Cell Biol.* **18**, 527-539 (2016).

87. C. L. Klaips, G. G. Jayaraj, F. U. Hartl, Pathways of cellular proteostasis in aging and disease. *J. Cell Biol.* **217**, 51-63 (2018).

88. M. H. Glickman, A. Ciechanover, The ubiquitin-proteasome proteolytic pathway: destruction for the sake of construction. *Physiol. Rev.* **82**, 373-428 (2002).

89. N. P. Dantuma, K. Lindsten, R. Glas, M. Jellne, M. G. Masucci, Short-lived green fluorescent proteins for quantifying ubiquitin/proteasome-dependent proteolysis in living cells. *Nat. Biotechnol.* **18**, 538-543 (2000).

90. D. S. Leeman, K. Hebestreit, T. Ruetz, A. E. Webb, A. McKay, E. A. Pollina, B. W. Dulken, X. Zhao, R. W. Yeo, T. T. Ho, S. Mahmoudi, K. Devarajan, E.

Passegue, T. A. Rando, J. Frydman, A. Brunet, Lysosome activation clears aggregates and enhances quiescent neural stem cell activation during aging. *Science* **359**, 1277-1283 (2018).

91. Y. Narain, A. Wyttenbach, J. Rankin, R. A. Furlong, D. C. Rubinsztein, A molecular investigation of true dominance in Huntington's disease. *J. Med. Genet.* **36**, 739-746 (1999).

92. E. Agathokleous, E. J. Calabrese, Hormesis: a general biological principle. *Chem. Res. Toxicol.* **35**, 547-549 (2022).

93. V. Schirrmacher, Less can be more: the hormesis theory of stress adaptation in the global biosphere and its implications. *Biomedicines* **9**, 293 (2021).

94. D. Gems, L. Partridge, Stress-response hormesis and aging: "that which does not kill us makes us stronger". *Cell Metab.* **7**, 200-203 (2008).

95. M. A. Mourao, J. B. Hakim, S. Schnell, Connecting the dots: the effects of macromolecular crowding on cell physiology. *Biophys. J.* **107**, 2761-2766 (2014).

96. M. Costa-Mattioli, P. Walter, The integrated stress response: From mechanism to disease. *Science* **368**, eaat5314 (2020).

97. I. Novoa, Y. Zhang, H. Zeng, R. Jungreis, H. P. Harding, D. Ron, Stress-induced gene expression requires programmed recovery from translational repression. *EMBO J.* **22**, 1180-1187 (2003).

98. A. Krzyzosiak, A. Sigurdardottir, L. Luh, M. Carrara, I. Das, K. Schneider, A. Bertolotti, Target-based discovery of an inhibitor of the regulatory phosphatase PPP1R15B. *Cell* **174**, 1216-1228 (2018).

99. M. Carrara, A. Sigurdardottir, A. Bertolotti, Decoding the selectivity of eIF2α holophosphatases and PPP1R15A inhibitors. *Nat. Struct. Mol. Biol.* **24**, 708-716 (2017).

100. X. Tian, S. Zhang, L. Zhou, A. A. Seyhan, L. Hernandez Borrero, Y. Zhang, W. S. El-Deiry, Targeting the integrated stress response in cancer therapy. *Front. Pharmacol.* **12**, 747837 (2021).

101. M. Delarue, G. P. Brittingham, S. Pfeffer, I. V. Surovtsev, S. Pinglay, K. J. Kennedy, M. Schaffer, J. I. Gutierrez, D. Sang, G. Poterewicz, J. K. Chung, J. M. Plitzko, J. T. Groves, C. Jacobs-Wagner, B. D. Engel, L. J. Holt, mTORC1 controls phase separation and the biophysical properties of the cytoplasm by tuning crowding. *Cell* **174**, 338-349 (2018).

102. A. Miermont, F. Waharte, S. Hu, M. N. McClean, S. Bottani, S. Leon, P. Hersen, Severe osmotic compression triggers a slowdown of intracellular signaling, which can be explained by molecular crowding. *Proc. Natl. Acad. Sci. USA* **110**, 5725-5730 (2013).

103. H. X. Zhou, G. Rivas, A. P. Minton, Macromolecular crowding and confinement: biochemical, biophysical, and potential physiological consequences. *Annu. Rev. Biophys.* **37**, 375-397 (2008).

104. V. Trappe, V. Prasad, L. Cipelletti, P. N. Segre, D. A. Weitz, Jamming phase diagram for attractive particles. *Nature* **411**, 772-775 (2001).

105. I. M. Kuznetsova, K. K. Turoverov, V. N. Uversky, What macromolecular crowding can do to a protein. *Int. J. Mol. Sci.* **15**, 23090-23140 (2014).

106. M. Sakamoto, T. Minamino, H. Toko, Y. Kayama, Y. Zou, M. Sano, E. Takaki, T. Aoyagi, K. Tojo, N. Tajima, A. Nakai, H. Aburatani, I. Komuro, Upregulation

of heat shock transcription factor 1 plays a critical role in adaptive cardiac hypertrophy. *Circ. Res.* **99**, 1411-1418 (2006).

107. T. Koya, S. Nishizawa, Y. Ohno, A. Goto, A. Ikuta, M. Suzuki, T. Ohira, T. Egawa, A. Nakai, T. Sugiura, Y. Ohira, T. Yoshioka, M. Beppu, K. Goto, Heat shock transcription factor 1-deficiency attenuates overloading-associated hypertrophy of mouse soleus muscle. *PLoS ONE* **8**, e77788 (2013).

108. S. Obi, T. Nakajima, T. Hasegawa, F. Nakamura, M. Sakuma, S. Toyoda, C. Tei, T. Inoue, Heat induces myogenic transcription factors of myoblast cells via transient receptor potential vanilloid 1 (Trpv1). *FEBS Open Bio* **9**, 101-113 (2019).

109. M. V. Blagosklonny, Rapamycin for longevity: opinion article. *Aging* **11**, 8048-8067 (2019).

110. I. Bjedov, J. M. Toivonen, F. Kerr, C. Slack, J. Jacobson, A. Foley, L. Partridge, Mechanisms of life span extension by rapamycin in the fruit fly Drosophila melanogaster. *Cell Metab.* **11**, 35-46 (2010).

111. M. Hansen, S. Taubert, D. Crawford, N. Libina, S. J. Lee, C. Kenyon, Lifespan extension by conditions that inhibit translation in *Caenorhabditis elegans*. *Aging Cell* **6**, 95-110 (2007).

112. C. Selman, J. M. Tullet, D. Wieser, E. Irvine, S. J. Lingard, A. I. Choudhury, M. Claret, H. Al-Qassab, D. Carmignac, F. Ramadani, A. Woods, I. C. Robinson, E. Schuster, R. L. Batterham, S. C. Kozma, G. Thomas, D. Carling, K. Okkenhaug, J. M. Thornton, L. Partridge, D. Gems, D. J. Withers, Ribosomal protein S6 kinase 1 signaling regulates mammalian life span. *Science* **326**, 140-144 (2009).

113. E. Bernal-Mizrachi, W. Wen, S. Stahlhut, C. M. Welling, M. A. Permutt, Islet β cell expression of constitutively active Akt1/PKBα induces striking hypertrophy, hyperplasia, and hyperinsulinemia. *J. Clin. Invest.* **108**, 1631-1638 (2001).

114. A. Milona, B. M. Owen, S. van Mil, D. Dormann, C. Mataki, M. Boudjelal, W. Cairns, K. Schoonjans, S. Milligan, M. Parker, R. White, C. Williamson, The normal mechanisms of pregnancy-induced liver growth are not maintained in mice lacking the bile acid sensor FXR. *Am. J. Physiol. Gastrointest. Liver Physiol.* **298**, G151-158 (2010).

115. F. Sinturel, A. Gerber, D. Mauvoisin, J. Wang, D. Gatfield, J. J. Stubblefield, C. B. Green, F. Gachon, U. Schibler, Diurnal oscillations in liver mass and cell size accompany ribosome assembly cycles. *Cell* **169**, 651-663 (2017).

116. D. Picard, E. Suslova, P. A. Briand, 2-color photobleaching experiments reveal distinct intracellular dynamics of two components of the Hsp90 complex. *Exp. Cell Res.* **312**, 3949-3958 (2006).

117. H. Reinke, C. Saini, F. Fleury-Olela, C. Dibner, I. J. Benjamin, U. Schibler, Differential display of DNA-binding proteins reveals heat-shock factor 1 as a circadian transcription factor. *Genes Dev.* **22**, 331-345 (2008).

118. E. Kirschke, D. Goswami, D. Southworth, P. R. Griffin, D. A. Agard, Glucocorticoid receptor function regulated by coordinated action of the Hsp90 and Hsp70 chaperone cycles. *Cell* **157**, 1685-1697 (2014).

119. K. N. Richter, N. H. Revelo, K. J. Seitz, M. S. Helm, D. Sarkar, R. S. Saleeb, E. D'Este, J. Eberle, E. Wagner, C. Vogl, D. F. Lazaro, F. Richter, J. Coy-Vergara, G. Coceano, E. S. Boyden, R. R. Duncan, S. W. Hell, M. A.

Lauterbach, S. E. Lehnart, T. Moser, T. F. Outeiro, P. Rehling, B. Schwappach, I. Testa, B. Zapiec, S. O. Rizzoli, Glyoxal as an alternative fixative to formaldehyde in immunostaining and super-resolution microscopy. *EMBO J.* **37**, 139-159 (2018).

120. N. A. Kulak, G. Pichler, I. Paron, N. Nagaraj, M. Mann, Minimal, encapsulated proteomic-sample processing applied to copy-number estimation in eukaryotic cells. *Nat. Methods* **11**, 319-324 (2014).

Acknowledgments

We are indebted to Manfredo Quadroni of the PAF of the University of Lausanne for the proteomic analyses. We are grateful to the Bioimaging Center of the Faculty of Science of the University of Geneva for assistance with the confocal microscopy.

Funding: This work has been supported by the Swiss National Science Foundation (grant 31003A_172789/1) and the Canton de Genève.

Author contributions: S.M. and D.P. conceived the study; S.M. designed and performed most of the experiments, analyzed most of the data, prepared the figures and wrote the drafts; K.B. contributed in designing some experiments, performed proteasome activity assays, and prepared figures; D.W. performed some Western blots; D.H. contributed in FRAP measurements and analysis; O.P performed the polysome profiling; L.B. did the cloning of shRNA constructs and their initial validation; N.H. contributed to the proteomic data analyses; D.P. supervised the work, contributed to the design of the experiments, wrote, and critically edited the manuscript. All authors have read and agreed to the published version of the manuscript.

Competing interests: Authors declare that they have no competing interests.

Data and materials availability: The mass spectrometry proteomics data are made available via ProteomeXchange with the identifier PXD039672, and for a subset,

they are available in data S1. All other data needed to evaluate the conclusions in the paper are presented in the paper, and/or the Supplementary Materials.

Figures and corresponding legends

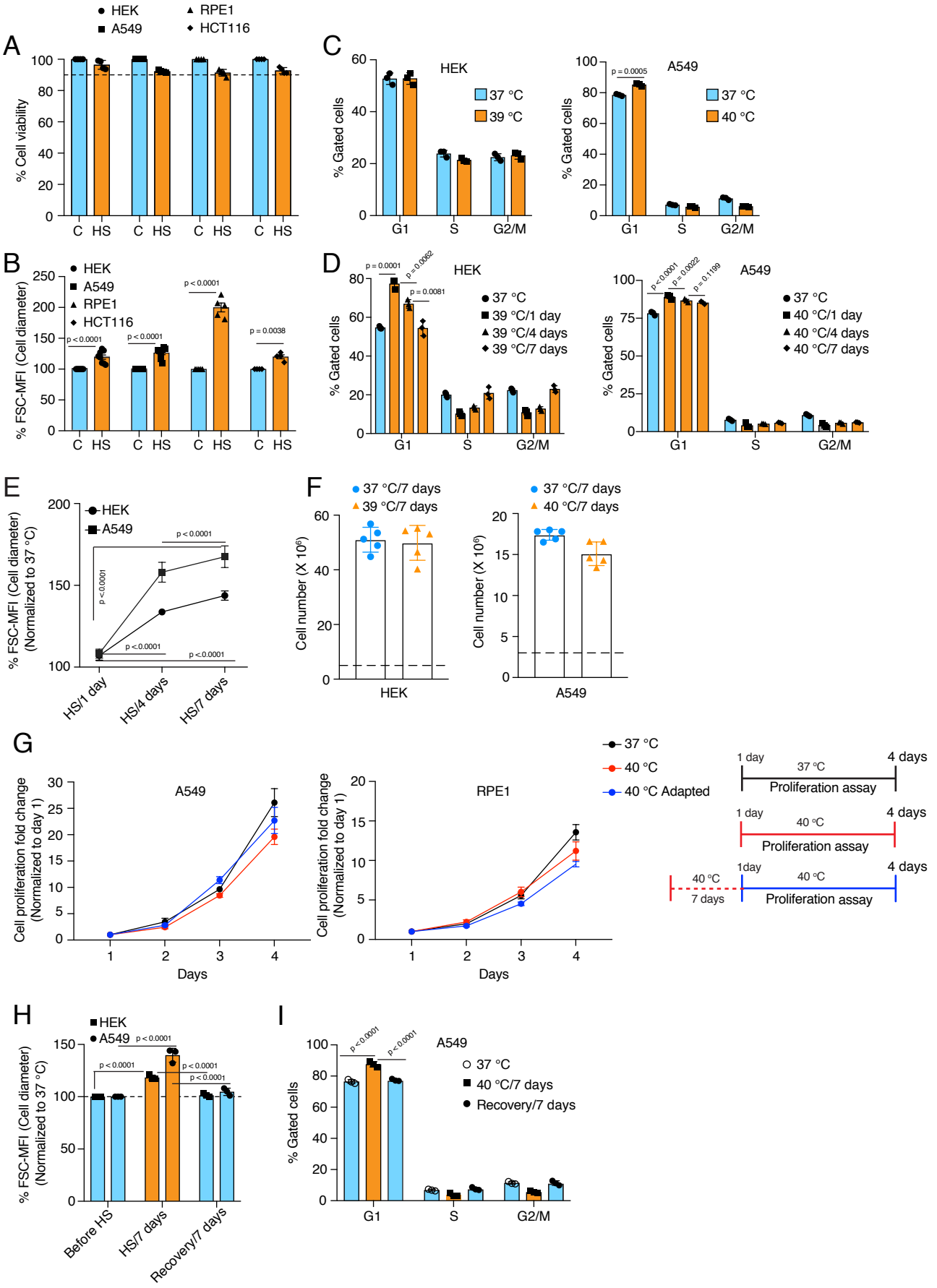
A
HEK
A549
RPE1
HCT116
% Cell viability
C HS C HS C HS C HS
B
% FSC-MFI (Cell diameter)
p < 0.0001
p = 0.0038
C
HEK
A549
37 °C
39 °C
40 °C
% Gated cells
p = 0.0005
G1
S
G2/M
D
p = 0.0001
p = 0.0082
p = 0.0081
p < 0.0001
p = 0.0022
p = 0.1199
37 °C
39 °C/1 day
39 °C/4 days
39 °C/7 days
40 °C/1 day
40 °C/4 days
40 °C/7 days
E
% FSC-MFI (Cell diameter) (Normalized to 37 °C)
HS/1 day
HS/4 days
HS/7 days
F
37 °C/7 days
39 °C/7 days
40 °C/7 days
Cell number (X 10^6)
G
A549
RPE1
Cell proliferation fold change (Normalized to day 1)
Days
37 °C
40 °C
40 °C Adapted
1 day
4 days
Proliferation assay
40 °C
7 days
1day
H
Before HS
HS/7 days
Recovery/7 days
I
Recovery/7 days

Fig. 1. Cells increase their size in response to chronic stress. (A) Flow cytometric quantification of cell viability under chronic HS for 7 days (HS = 39°C for HEK and HCT116 cells; HS = 40 °C for A549 and RPE1 cells) (n = 4 biologically independent samples). **(B)** Flow cytometric quantification of cell size after 7 days of chronic HS (biologically independent samples: n = 6 for HEK and A549; n = 5 for RPE1; n = 4 for HCT116). **(C** and **D)** Flow cytometric analysis of cell cycle (n = 3 biologically independent samples). **(E)** Flow cytometric quantification of cell size during different time intervals of chronic HS (n = 4 biologically independent samples). **(F)** Proliferation of HEK and A549 cells at the indicated temperature for the indicated period presented as cell numbers. Cells were seeded at a density of 5 x 10^6 and 3 x 10^6 per 15 cm plate for HEK and A549 cells, respectively. The numbers of live cells counted after 7 days are plotted (n = 5 biologically independent experiments). **(G)** Proliferation of A549 and RPE1 cells measured with a crystal violet assay (n = 3 biologically independent experiments). The adapted cells were maintained at 40 °C for one week before this experimental start point and continued at 40 °C during the experiment. See scheme of the experiment on the right. **(H)** Flow cytometric quantification of cell size in chronic HS and recovery (n = 3 biologically independent samples). (**I)** Flow cytometric analysis of cell cycle in chronic HS and post HS recovery (n = 3 biologically independent samples). The data are represented as mean values ± SEM for all bar and line graphs. The statistical significance between the groups was analyzed by two-tailed unpaired Student's t-tests.

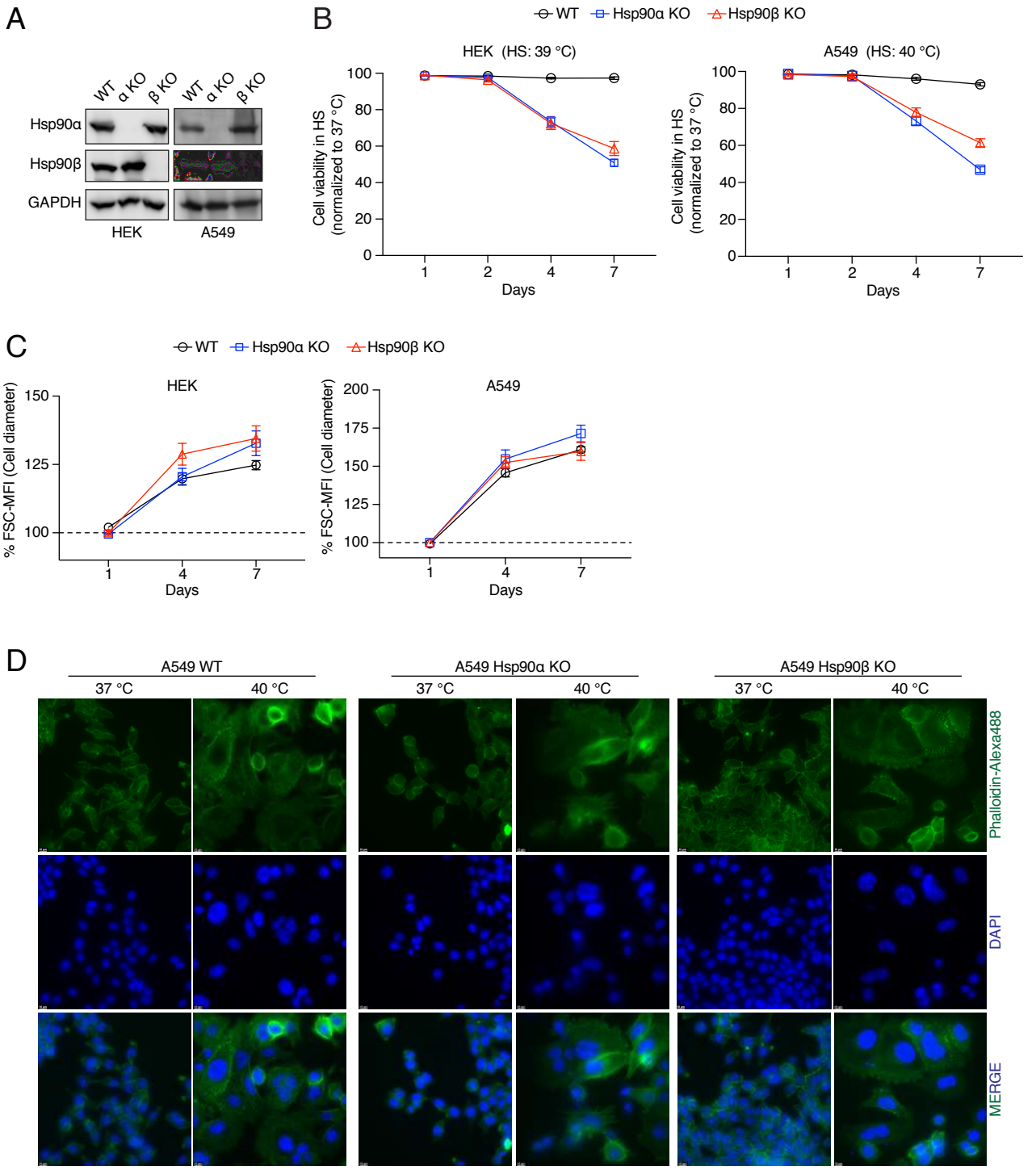
A
WT
α KO
β KO
WT
α KO
β KO
Hsp90α
Hsp90β
GAPDH
HEK
A549
B
WT
Hsp90α KO
Hsp90β KO
HEK (HS: 39 °C)
A549 (HS: 40 °C)
Cell viability in HS (normalized to 37 °C)
Days
C
WT
Hsp90α KO
Hsp90β KO
HEK
A549
% FSC-MFI (Cell diameter)
Days
D
A549 WT
A549 Hsp90α KO
A549 Hsp90β KO
37 °C
40 °C
Phalloidin-Alexa488
DAPI
MERGE

Fig. 2. **Cells are unable to adapt to chronic stress in the absence of one of the cytosolic Hsp90 isoforms. (A)** Immunoblots of Hsp90α and Hsp90β in WT HEK and A549 cells, and their respective Hsp90α/β KO cells. GAPDH serves as the loading control (α KO; Hsp90α KO and β KO; Hsp90β KO) (representative images of n = 4 biologically independent experiments). **(B)** Flow cytometric quantification of cell viability of HEK, A549, and their respective Hsp90α/β KO cells in chronic HS at different time points during a period of 7 days (n = 5 biologically independent samples). Note that the X axis does not have a linear scale and that lines connecting the data points are drawn as a visual aid. **(C)** Flow cytometric quantification of cell size in chronic HS at different time points during a period of 7 days (HS = 39 °C for HEK and 40 °C for A549) (n = 4 biologically independent samples) The data are represented as mean values ± SEM for all bar graphs. The statistical significance between the groups was analyzed by two-tailed unpaired Student's t-tests. **(D)** Fluorescence microscopy images of A549 WT and Hsp90α/β KO cells after 4 days of chronic HS. The cytoskeleton is stained with phalloidin-Alexa488 (green), and the nucleus is stained with DAPI (blue). Images were captured with a fluorescence microscope (Zeiss, Germany). The scale bar on the images is 10 μM (images are representative of n = 2 biologically independent experiments).

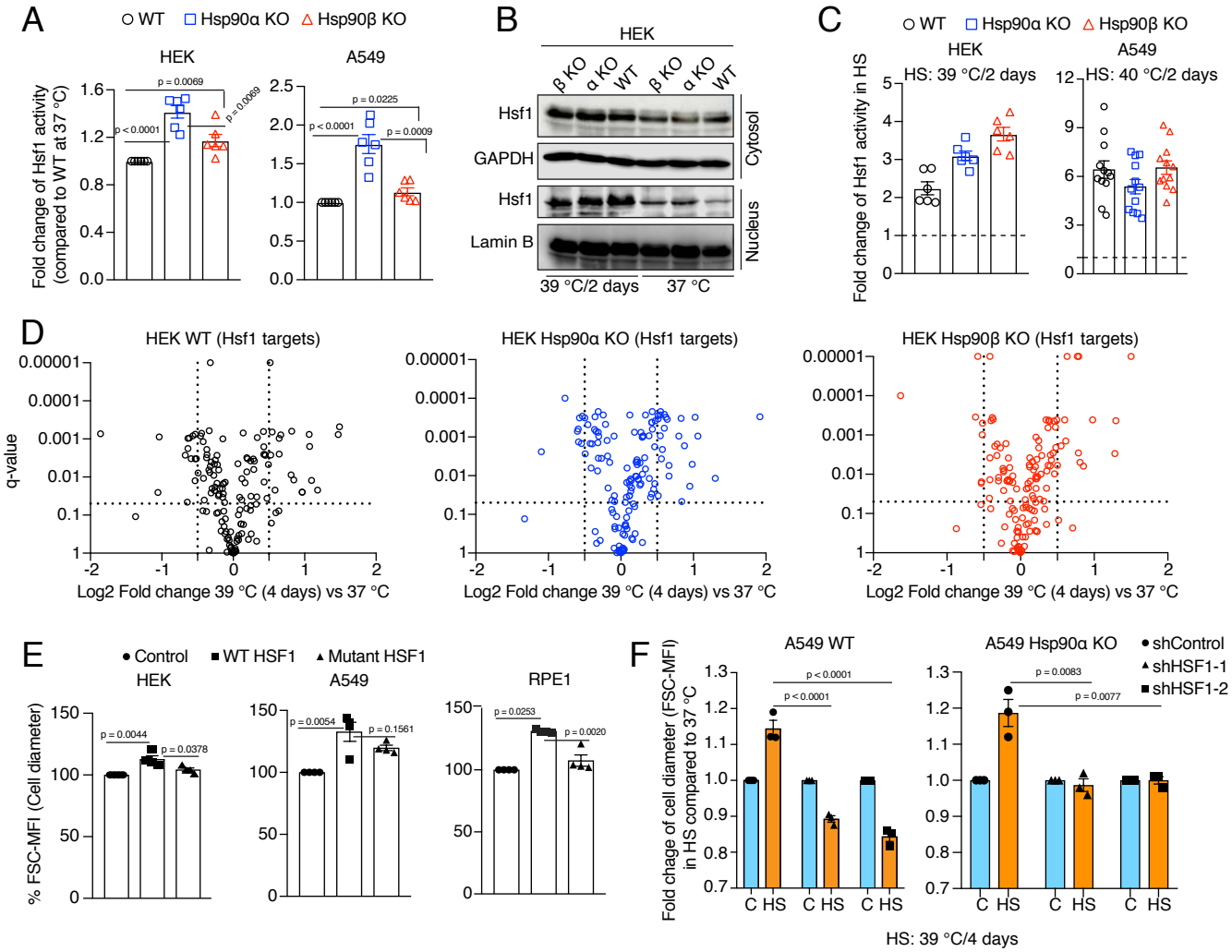
A
WT
Hsp90α KO
Hsp90β KO
HEK
A549
Fold change of Hsf1 activity (compared to WT at 37 °C)
p = 0.0069
p < 0.0001
p = 0.0069
p = 0.0225
p < 0.0001
p = 0.0009
B
HEK
β KO
α KO
WT
β KO
α KO
WT
Hsf1
GAPDH
Hsf1
Lamin B
Cytosol
Nucleus
39 °C/2 days
37 °C
C
WT
Hsp90α KO
Hsp90β KO
HEK
HS: 39 °C/2 days
A549
HS: 40 °C/2 days
Fold change of Hsf1 activity in HS
D
HEK WT (Hsf1 targets)
HEK Hsp90α KO (Hsf1 targets)
HEK Hsp90β KO (Hsf1 targets)
q-value
Log2 Fold change 39 °C (4 days) vs 37 °C
E
Control
WT HSF1
Mutant HSF1
HEK
A549
RPE1
% FSC-MFI (Cell diameter)
p = 0.0044
p = 0.0378
p = 0.0054
p = 0.1561
p = 0.0253
p = 0.0020
F
A549 WT
A549 Hsp90α KO
shControl
shHSF1-1
shHSF1-2
Fold chage of cell diameter (FSC-MFI) in HS compared to 37 °C
p < 0.0001
p < 0.0001
p = 0.0083
p = 0.0077
C HS C HS C HS
HS: 39 °C/4 days

Fig. 3. Hsf1 regulates cell size in response to stress. (A) Fold change of Hsf1 activity of HEK WT, A549 WT, and their respective Hsp90α/β KO cells at 37 °C as measured by luciferase reporter assay (n = 3 biologically independent samples and 2 experimental replicates each time). (**B**) Immunoblots of Hsf1 in the cytosolic and nuclear fractions of HEK WT and Hsp90α/β KO cells (α KO, Hsp90αKO; β KO, Hsp90βKO). GAPDH and lamin B1 serve as loading controls (representative blots of n = 2 biologically independent experiments). (**C)** Fold change of Hsf1 activity of HEK WT, A549 WT, and their respective Hsp90α/β KO cells in chronic HS as measured by luciferase reporter assay (n = 3 biologically independent samples, and 2 experimental replicates each time for HEK; n = 3 biologically independent samples, and 4 experimental replicates each time for A549). **(D)** Volcano plots of the normalized fold changes in protein levels of some core Hsf1 target genes (list obtained from https://hsf1base.org/) in chronic HS, determined by quantitative label-free proteomic analysis of Hsp90α/β KO and WT HEK cells. Molecular chaperones, whose expression is regulated by Hsf1, are excluded from this dataset. Each genotype was compared with its respective 37 °C control (n = 3 biologically independent samples). Log2 fold changes of > 0.5 or < -0.5 with a p-value of < 0.05 were considered significant differences for a particular protein. **(E)** Flow cytometric quantification of cell size of HEK, A549, and RPE1 cells upon overexpression of WT Hsf1 (with plasmid pcDNA-Flag HSF1 wt) or mutant Hsf1 (pcDNA-Flag HSF1 C205, retaining the first 205 amino acids), and with plasmid pcDNA3.1(+) as empty vector control. Transfected cells to be measured were identified on the basis of their coexpression of EGFP (n = 4 biologically independent experiments). **(F)** Flow cytometric quantification of cell size in chronic HS after knockdown of Hsf1 in A549

WT and Hsp90αKO cells. Here the chronic HS for A549 cells is at 39 °C instead of 40 °C to reduce HS-induced damage in Hsf1 knockdown conditions (n = 3 biologically independent samples). **(G)** Flow cytometric quantification of cell cycle in HS after knockdown of Hsf1 in A549 WT and Hsp90αKO cells. The data are represented as mean values ± SEM for all bar graphs. The statistical significance between the groups was analyzed by two-tailed unpaired Student's t-tests.

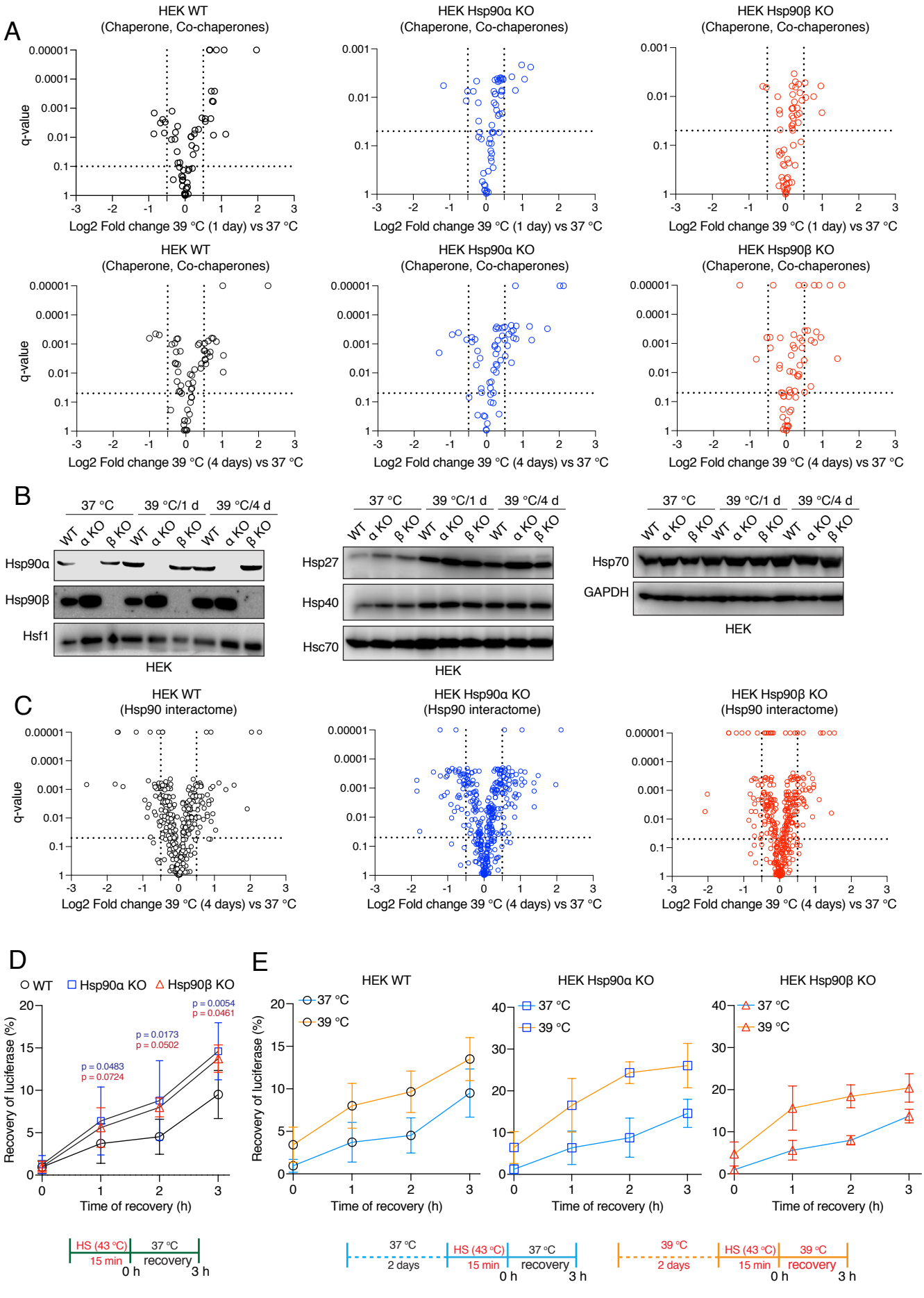
A
HEK WT
(Chaperone, Co-chaperones)
HEK Hsp90α KO
(Chaperone, Co-chaperones)
HEK Hsp90β KO
(Chaperone, Co-chaperones)
q-value
Log2 Fold change 39 °C (1 day) vs 37 °C
Log2 Fold change 39 °C (4 days) vs 37 °C
B
37 °C
39 °C/1 d
39 °C/4 d
WT
α KO
β KO
Hsp90α
Hsp90β
Hsf1
HEK
Hsp27
Hsp40
Hsc70
Hsp70
GAPDH
C
HEK WT
(Hsp90 interactome)
HEK Hsp90α KO
(Hsp90 interactome)
HEK Hsp90β KO
(Hsp90 interactome)
D
WT
Hsp90α KO
Hsp90β KO
p = 0.0054
p = 0.0461
p = 0.0173
p = 0.0502
p = 0.0483
p = 0.0724
Recovery of luciferase (%)
Time of recovery (h)
HS (43 °C)
15 min
37 °C
recovery
0 h
3 h
E
37 °C
39 °C
2 days

Fig. 4. Hsp90α/β KO cells maintain chaperones, co-chaperones, and Hsp90 interactors during chronic stress adaptation. (A) Volcano plots of the normalized fold changes of molecular chaperones and co-chaperones of cells subjected to 1 and 4 days of chronic HS determined by quantitative label-free proteomic analysis of Hsp90α/β KO and WT HEK cells. Each genotype was compared with its respective 37 °C control (*n* = 3 biologically independent samples)**. (B)** Immunoblots of different molecular chaperones in HEK WT and Hsp90α/β KO cells (α KO, Hsp90αKO; β KO, Hsp90βKO). GAPDH serves as the loading control for all three panels (representative of n = 2 independent experiments). **(C)** Volcano plots of the normalized fold changes of Hsp90 interactors (list obtained from https://www.picard.ch/Hsp90Int) in 4 days of chronic HS determined by quantitative label-free proteomic analysis of Hsp90α/β KO and WT HEK cells. Each genotype was compared with its respective 37 °C control (n = 3 biologically independent samples). For all volcano plots, Log2 fold changes of > 0.5 or < -0.5 with a p-value of < 0.05 were considered significant differences for a particular protein. **(D** and **E)** *In vivo* refolding of heat-denatured luciferase of control cells (blue line) and cells heat-adapted to 39 °C (orange line). Luciferase activity before the acute HS (at 43 °C) is set to 100% (n = 3 biologically independent samples). See scheme of the experiment below. Note the different scales of the Y axes of the bar graphs in panel E. The data are represented as mean values ± SEM for all bar graphs. The statistical significance between the groups was analyzed by two-tailed unpaired Student's t-tests. The p-values for Hsp90α and Hsp90β KO cells are in blue and red, respectively. All the p-values are for comparisons to the respective WT.

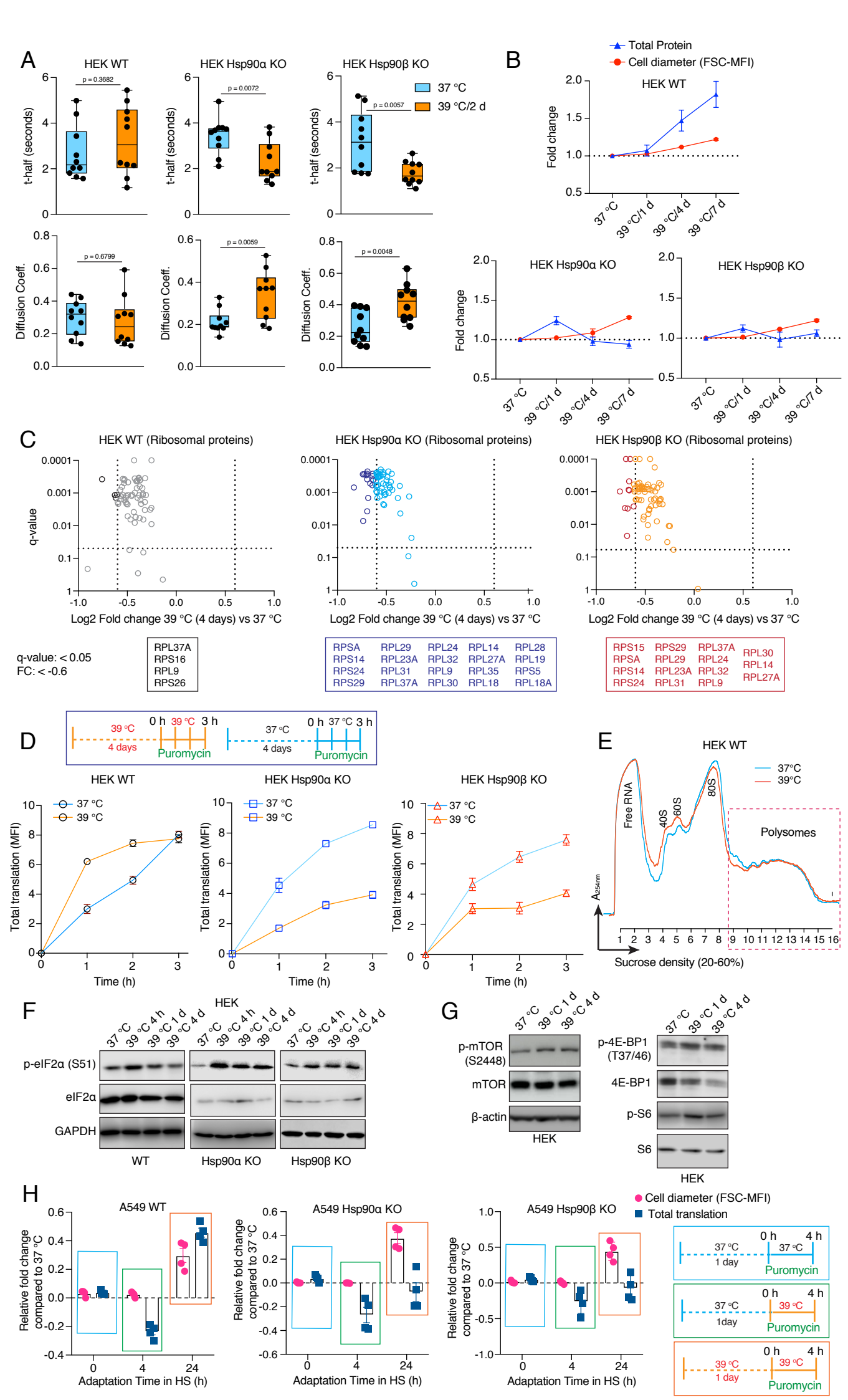
A
HEK WT
HEK Hsp90α KO
HEK Hsp90β KO
37 °C
39 °C/2 d
t-half (seconds)
Diffusion Coeff.
p = 0.3682
p = 0.0072
p = 0.0057
p = 0.6799
p = 0.0059
p = 0.0048
B
Total Protein
Cell diameter (FSC-MFI)
Fold change
37 °C
39 °C/1 d
39 °C/4 d
39 °C/7 d
C
HEK WT (Ribosomal proteins)
HEK Hsp90α KO (Ribosomal proteins)
HEK Hsp90β KO (Ribosomal proteins)
q-value
Log2 Fold change 39 °C (4 days) vs 37 °C
q-value: < 0.05
FC: < -0.6
RPL37A
RPS16
RPL9
RPS26
RPSA RPL29 RPL24 RPL14 RPL28
RPS14 RPL23A RPL32 RPL27A RPL19
RPS24 RPL31 RPL9 RPL35 RPS5
RPS29 RPL37A RPL30 RPL18 RPL18A
RPS15 RPS29 RPL37A
RPSA RPL29 RPL24 RPL30
RPS14 RPL23A RPL32 RPL14
RPS24 RPL31 RPL9 RPL27A
D
39 °C
4 days
0 h
3 h
Puromycin
37 °C
HEK WT
HEK Hsp90α KO
HEK Hsp90β KO
Total translation (MFI)
Time (h)
E
HEK WT
37°C
39°C
Free RNA
40S
60S
80S
Polysomes
Sucrose density (20-60%)
F
HEK
37 °C
39 °C 4 h
39 °C 1 d
39 °C 4 d
p-eIF2α (S51)
eIF2α
GAPDH
WT
Hsp90α KO
Hsp90β KO
G
p-mTOR (S2448)
mTOR
β-actin
HEK
p-4E-BP1 (T37/46)
4E-BP1
p-S6
S6
H
A549 WT
A549 Hsp90α KO
A549 Hsp90β KO
Cell diameter (FSC-MFI)
Total translation
Relative fold change compared to 37 °C
Adaptation Time in HS (h)
37 °C
1 day
39 °C
1day
Puromycin

Fig. 5. Hsp90α/β KO cells suffer from cytoplasmic protein dilution during adaptation to chronic stress. (A) FRAP experiments with control and heat-adapted live cells expressing EGFP. The respective box plots show the t-half values of recovery of EGFP fluorescence and the apparent EGFP diffusion coefficients (n= 10 cells from 2 biologically independent experiments). **(B)** Fold change of cell size (represented by the FSC-MFI values) and total proteins (determined as MFI-FL1 values) in chronic HS as analyzed by flow cytometry. Cells were fixed, and total proteins were stained using Alexa Fluor 488 NHS ester (n = 3 biologically independent experiments). Lines connecting the data points are drawn as a visual aid. **(C)** Volcano plots of the normalized fold changes of the ribosomal proteins (list obtained from http://ribosome.med.miyazaki-u.ac.jp/) after 4 days of chronic HS determined by quantitative label-free proteomic analysis in Hsp90α/β KO and WT HEK cells. Each genotype was compared with its respective 37 °C control (n= 3 biologically independent samples). Log2 fold changes of > 0.6 or < -0.6 with a p-value of < 0.05 were considered significant differences for a particular protein. The box below the volcano plot shows the corresponding names of the proteins that were significantly downregulated. **(D)** Flow cytometric analysis of total translation of HEK WT and Hsp90α/β KO cells at 37 °C and after 4 days of chronic HS (see scheme of the experiment on the top). Nascent polypeptide chains were labeled with OP-puromycin during cell culture, and the incorporation of puromycin at different time points was analyzed (n = 4 experimental samples). **(E)** Representative polysome profiles of HEK WT cells at 37 °C and after 4 days of chronic HS (representative of n = 2 biologically independent experiments). **(F** and **G)** Immunoblots of some of the translation-related proteins. GAPDH and β-actin serve as loading controls (images

are representative of n = 2 independent biological samples). **(H)** Relative fold changes of total translation and cell size in the early phase of adaptation to chronic HS (see schemes of experiments on the right) for A549 WT and Hsp90α/β KO cells**.** The data are represented as mean values ± SEM for all bar graphs. The statistical significance between the groups was analyzed by two-tailed unpaired Student's t-tests.

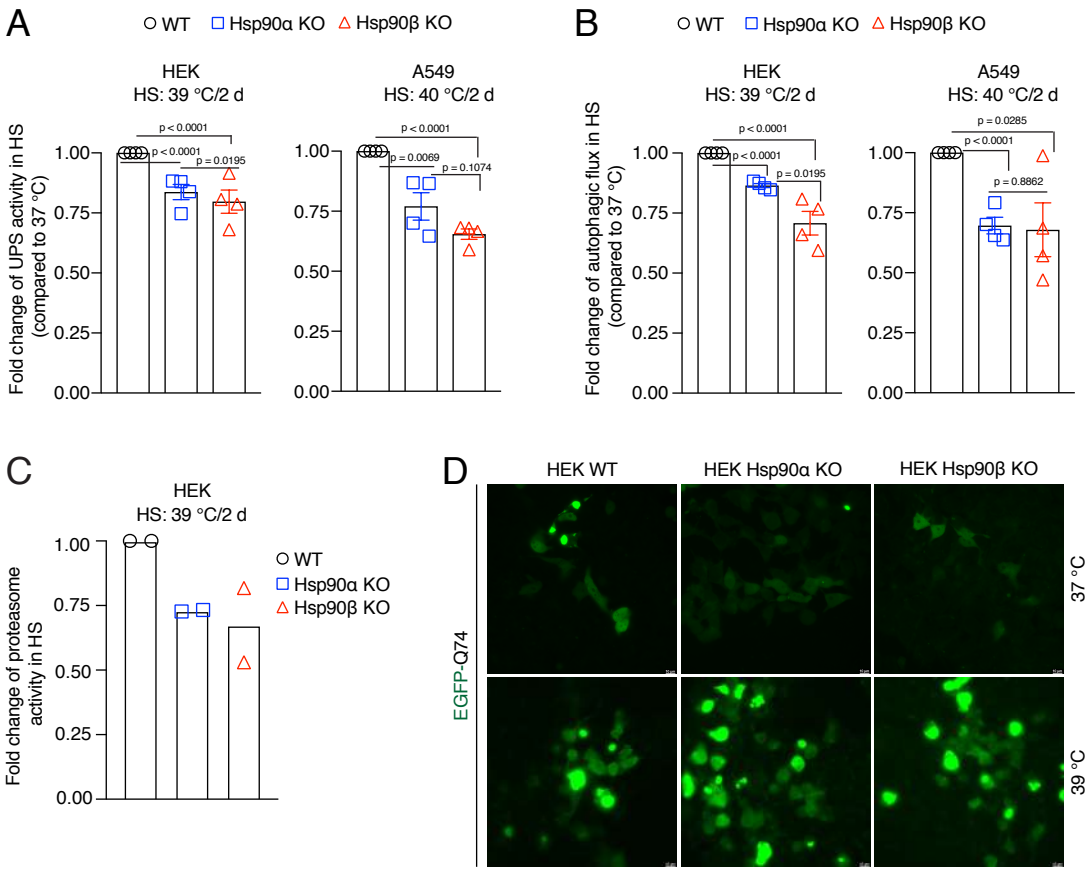
A
WT
Hsp90α KO
Hsp90β KO
HEK
HS: 39 °C/2 d
A549
HS: 40 °C/2 d
Fold change of UPS activity in HS (compared to 37 °C)
p < 0.0001
p < 0.0001
p = 0.0195
p < 0.0001
p = 0.0069
p = 0.1074
1.00
0.75
0.50
0.25
0.00
B
Fold change of autophagic flux in HS (compared to 37 °C)
p < 0.0001
p < 0.0001
p = 0.0195
p = 0.0285
p < 0.0001
p = 0.8862
C
Fold change of proteasome activity in HS
D
HEK WT
HEK Hsp90α KO
HEK Hsp90β KO
EGFP-Q74
37 °C
39 °C

Fig. 6. Hsp90 is crucial for cellular proteostasis during adaptation to chronic stress. (A) Flow cytometric determination of the *in vivo* UPS activity in chronic HS compared to 37 °C, using the Ub-M-GFP and Ub-R-GFP reporter proteins (n = 4 biologically independent samples). **(B)** Flow cytometric measurement of autophagic flux in chronic HS compared to 37 °C, using a mCherry-GFP-LC3 reporter. Flux is calculated as the ratio of the mean fluorescence intensities of mCherry and GFP-positive cells (n = 4 biologically independent samples). **(C)** *In vitro* steady-state proteasomal activity with lysates of HEK WT, and Hsp90α and Hsp90β KO cells determined by measuring fluorescence of the cleaved substrate suc-LLVY-AMC (n = 2 biologically independent samples). **(D)** Fluorescence micrographs of cells expressing the fusion protein EGFP-Q74 visible as aggregates with green fluorescence. The scale bar in micrographs indicates 10 µm (images are representative of n = 2 independent biological samples). The data are represented as mean values ± SEM for all bar graphs. The statistical significance between the groups was analyzed by two-tailed unpaired Student's t-tests.

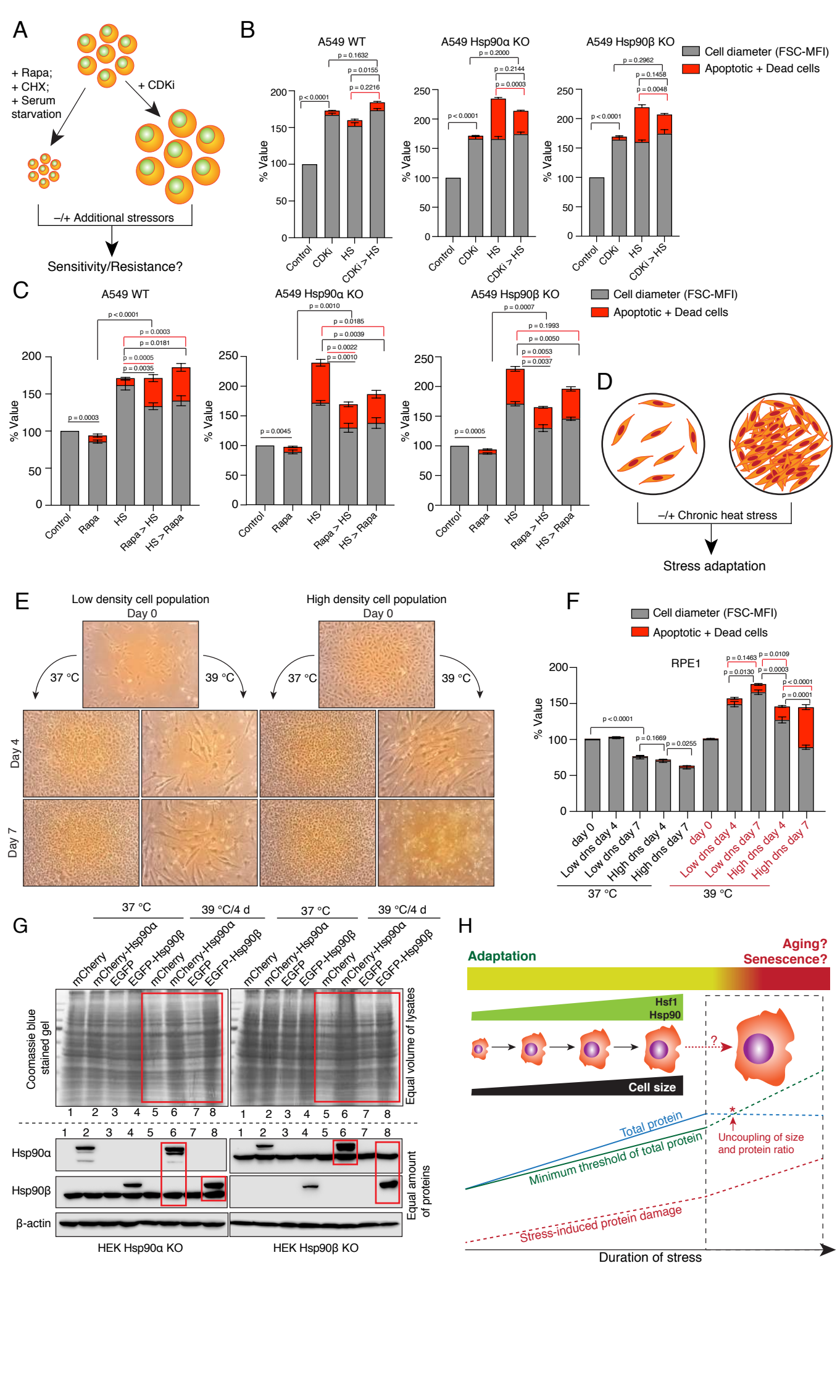
A
+ Rapa;
+ CHX;
+ Serum
starvation
+ CDKi
–/+ Additional stressors
Sensitivity/Resistance?
B
A549 WT
A549 Hsp90α KO
A549 Hsp90β KO
Cell diameter (FSC-MFI)
Apoptotic + Dead cells
% Value
Control
CDKi
HS
CDKi > HS
C
A549 WT
A549 Hsp90α KO
A549 Hsp90β KO
Cell diameter (FSC-MFI)
Apoptotic + Dead cells
% Value
Control
Rapa
HS
Rapa > HS
HS > Rapa
D
–/+ Chronic heat stress
Stress adaptation
E
Low density cell population
Day 0
High density cell population
Day 0
37 °C
39 °C
Day 4
Day 7
F
Cell diameter (FSC-MFI)
Apoptotic + Dead cells
RPE1
% Value
day 0
Low dns day 4
Low dns day 7
High dns day 4
High dns day 7
37 °C
39 °C
G
37 °C
39 °C/4 d
mCherry
mCherry-Hsp90α
EGFP
EGFP-Hsp90β
Coomassie blue stained gel
Equal volume of lysates
Hsp90α
Hsp90β
β-actin
Equal amount of proteins
HEK Hsp90α KO
HEK Hsp90β KO
H
Adaptation
Aging?
Senescence?
Hsf1
Hsp90
Cell size
Total protein
Minimum threshold of total protein
Uncoupling of size and protein ratio
Stress-induced protein damage
Duration of stress

Fig. 7. Enlarged cells are more resistant to additional stress. (A) Scheme of cell size enlargement or reduction experiments. CHX, cycloheximide; CDKi, CDK4/6 inhibitor. **(B)** Cell size was first enlarged by treating cells with 100 nM CDKi for 3 days; then, cells were washed and subjected to chronic HS at 40 °C for 3 more days (CDKi > HS). Cell size (% FSC-MFI; grey part of the bars) and cell death (% annexin V and PI-positive; red part of the bars) were measured by flow cytometry. The values for cell size and death in the different experimental conditions are normalized to the respective 37 °C controls (n = 3 biologically independent experiments). **(C)** Cells were first pretreated with 7.5 nM rapamycin (Rapa) for 3 days to reduce the cell size. After that, the cells were subjected to chronic HS at 40 °C for 3 days (Rapa > HS). HS > Rapa, the two treatments were done the other way around. The cell size (% FSC-MFI) and relative cell death (% annexin V and PI-positive) were quantified by flow cytometry. The values for cell size and death in different experimental conditions are normalized to the respective 37 °C control (n = 3 biologically independent experiments). **(D)** Scheme of experiments aimed at determining impact of limiting physical space on cell size increase. **(E** and **F)** Phase-contrast micrographs of RPE1 cells seeded in different numbers to restrict the space for cell size increase during adaptation to chronic HS (representative images of n = 4 biologically independent experiments). The cell size (% FSC-MFI) and relative cell death (% annexin V-PI positive) are quantified by flow cytometry. For the bar graphs, the values for cell size and death in different conditions are normalized to the low density (dns) cell population at 37 °C day 0 (n = 4 biologically independent experiments). The data are represented as mean values ± SEM for all bar graphs. **(G)** Immunoblots in the lower panels show the endogenous Hsp90α and Hsp90β, and the exogenously

overexpressed larger fusion proteins of Hsp90α (as mCherry-Hsp90α) and Hsp90β (as EGFP-Hsp90β), with red boxes highlighting samples with exogenous Hsp90. Images of the Coomassie-stained gels in the upper panels show the corresponding levels of total proteins with red boxes indicating lanes for samples from cells subjected to chronic HS (representative images of n = 2 biologically independent experiments). **(H)** Schematic representation of impact of chronic mild stress on cells. Wild-type cells initially adapt by enlarging their size and increasing total protein to maintain a minimum threshold level of functional proteins. The right part of the scheme (surrounded by a stippled box), shows what may happen if stress persists for much longer: cell size enlargement and translation are uncoupled, and because of protein damage, which continues to accumulate, cells become senescent and/or die.